Aalto-yliopisto
Aalto-universitetet
Aalto University

Master's Programme in Manufacturing

Optimizing Cylindricity Measurement Accuracy: Error Sources Analysis and Error Compensation Strategies in Calibration Labs

Honglei Xu

Master's thesis
2024

Copyright ©2024 Honglei Xu

Aalto-yliopisto
Aalto-universitetet
Aalto University

Author Honglei Xu

Title of thesis Optimizing Cylindricity Measurement Accuracy: Error Sources Analysis and Error Compensation Strategies in Calibration Labs

Programme Master's Programme in Manufacturing

Major Zero Defect Manufacture for a Circular Economy

Thesis supervisor Prof. Jouni Partanen

Thesis advisor(s) Dr Björn Hemming, Dr Pezhman Ghadimi

Collaborative partner VTT MIKES

Date 28.05.2024 **Number of pages** 55 + 16 **Language** English

Abstract

Cylindricity, a critical parameter in mechanical engineering, ensures the quality of rotary components. The cylindricity measuring machine in a calibration laboratory is dedicated to accurately measuring the straightness and roundness of cylindrical objects. A traditional cylindricity measuring machine consists of a rotary table, a stylus, and a column and arm for guiding vertical and horizontal movement. This thesis aims to enhance the accuracy of cylindricity measurements in laboratory settings.

Four key error sources were identified: rotary table error, probe precision, parallelism error, and straightness error. To quantify these error sources, five types of measurements were conducted according to the ISO 17025:2017 and ISO 9001:2015. The measured results were then compared with the manufacturer's specification. Importantly, MATLAB scripts were also employed to analyse and compensate for these errors.

Results show that while the rotary table error meets specifications and probe precision is acceptable, parallelism error and straightness error exceed them. However, compensation techniques can be applied for parallelism error and straightness error, significantly reducing instrument contribution to measured cylindricity error. Finally, measurement uncertainty was evaluated both with and without error compensation, demonstrating a notable reduction when compensation techniques were applied.

The insights gained will be applied to future cylindricity measurements at VTT MIKES, with accompanying instructions recorded in the institute's instructional materials. The findings also offer practical solutions for improving cylindricity measurements in calibration laboratories, contributing to the field's ongoing refinement and development.

Keywords Metrology, Calibration, Uncertainty, Roundness, Straightness, Cylindricity error, Error separation

Table of contents

Preface and acknowledgements

This thesis was prepared by using Taylor Hobson cylindricity measuring machine in the laboratory 010Pit of VTT MIKES. The thesis work is in the field of dimensional metrology including topics such as error separation methods, traceability, and uncertainty evaluation for high accuracy cylindricity measurements in the laboratory.

I extend my deepest gratitude to VTT MIKES for providing invaluable support and resources throughout the execution of this thesis. Their commitment to improving metrology research helped a lot with finishing this project.

I extend my gratitude to my thesis advisor, Dr. Björn Hemming, as well as to my thesis supervisors, Prof. Jouni Partanen from Aalto University and Dr Pezhman Ghadimi from University College Dublin, for their good advice and guidance. I want to convey my sincere gratitude to the head of our research group, Dr. Antti Lassila, for entrusting me with the subject of my master's thesis within the research endeavour, and for extending guidance and assistance.

I would like to thank MSc Ilkka Iisakka and Dr Richard Högström for offering the course on Measurement Uncertainty which has enriched my understanding of the foundations of metrology.

I am also grateful for all the colleagues who directly and indirectly supported me and the project, especially Dr Virpi Korpelainen, MSc Linus Teir, Dr Bruno Sauvet, MSc Aleksi Mattila, and MSc Ville Byman.

Lastly, I express gratitude to my family and friends for their accompany and encouragement.

Espoo, 28 May 2024

Honglei Xu

Digitally signed by Honglei Xu
DN: cn=Honglei Xu, o=Aalto University, email=honglei.xu@aalto.fi, c=FI
Date: 2024.05.28 14:35:09 +03'00'

Honglei Xu

Symbols and abbreviations

Symbols

 Cylindricity

 Roundness

 Flatness

 Straightness

Abbreviations

VTT	VTT Technical Research Centre of Finland
MIKES	Mittatekniikan keskus
ISO	International Organization for Standardization
SI	Système International
GPS	Geometrical product specifications
BIPM	Bureau international des poids et mesures
RONt	Peak-to-valley roundness deviation
FLTt	Peak-to-valley flatness deviation
CYLt	Peak-to-valley cylindricity deviation
STRt	Peak-to-valley straightness deviation
LS	Least Squares
LSCI	Least squares reference circle
LSCY	Least squares reference cylinder
MZ	Minimum Zone
MZCI	Minimum zone reference circle
MZCY	Minimum zone reference cylinder

1 Introduction

Cylindricity is a measure of how straight and round of a form. It plays a pivotal role in ensuring the manufacturing quality of rotary components in mechanical engineering, such as paper machine rolls, drivetrain shafts and many others. The precision in machining these parts directly influence the accuracy of subsequent assembly, which greatly effects on the overall machine quality. (Yang *et al.*, 2023). To ensure quality, the cylindricity measurements are needed.

A cylindricity measuring instrument is a device utilized to determine the measurement of straightness and roundness, as illustrated in Figure 1.1. Contact-type cylindricity measuring machines are commonly employed, where the stylus's tip is positioned to contact the object under the measurement. Subsequently, the object is rotated to take measurements. The resulting shape is obtained and cylindricity is calculated based on the collected data from different planes.

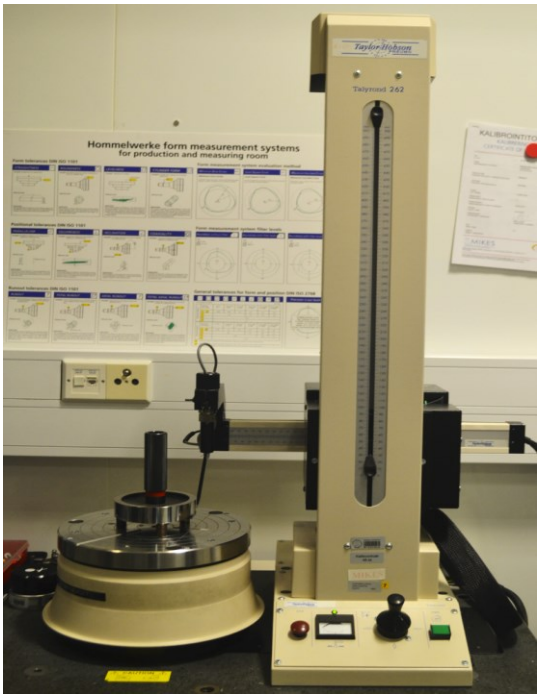

Figure 1.1: A cylindricity measuring machine measuring a plug gauge.

To ensure accuracy of cylindricity measurements, it is important to understand and consider the contribution of errors from the cylindricity measurement. While radial and axial errors of the rotary table are commonly recognized, it is crucial to evaluate the parallelism between the spindle and column

axes. This approach ensures comprehensive mitigation of potential sources of deviation, enhancing the overall precision of cylindricity measurements.

1.1 Research Problem

- What are the error sources in cylindricity measurement in a calibration laboratory and how can they be quantified?
- How can the influence of error sources in cylindricity measurement be minimized using error separation?

1.2 Goal

The goal of this thesis is to enhance the accuracy of cylindricity measurements in calibration laboratory settings by employing error separation methods, ensuring traceability, and evaluating uncertainty. This involves identifying, quantifying, and compensating for key error sources to minimize the instrument's contribution to measured cylindricity error.

1.3 Scope

This thesis was created for VTT MIKES, Finland's national metrology institute. It is a part of maintaining characterization and developing measurement capability of cylindricity, complying with the standards ISO 17025:2017 and ISO 9001:2015. The characterization is done using available known reference pieces (reference standard).

1.4 Outline

The paper is structured into four parts. The first part is an examination of fundamental metrology to provide an overview for subsequent sections. Cylindricity, calibration and cylindricity deviations are described in this part. The second part details the instrument, reference pieces, measurement processes, and the methodology employed for conducting the measurements. The following part is results which compares the measurement results with the manufacturer’s specification, the compensations of angle and straightness errors, and the evaluations of measurement uncertainty for cylindricity. Finally, the conclusion part synthesizes the main findings on error sources and compensation methods in cylindricity measurements, offering practical solutions for enhanced accuracy in calibration laboratories.

2 Literature review

2.1 Metrology

Metrology, science of measurement, holds significant importance in various fields by ensuring accuracy, consistency, and reliability in measurements. It consists of three primary activities that contribute to its significance in scientific and industrial domains. Firstly, metrology defines internationally accepted units of measurement across diverse applications, such as the metre. Secondly, the realization of these units employs scientific methods, such as lasers used in realizing a metre. Thirdly, metrology is pivotal in establishing traceability chains, documenting and disseminating the value and accuracy of measurements. For example, the relationship is established between the micrometre screw utilized in a precision engineering workshop and the primary laboratory specializing in optical length metrology.

Metrology further is divided into three categories based on its application - scientific, industrial, and legal metrology. Scientific metrology, positioned at the highest level of accuracy, is concerned with defining measurement standards. Industrial metrology, on the other hand, is focused on maintaining the optimal function of instruments used in industrial processes. Knowledge of measurement uncertainty is important in quality control of manufactured products. Finally, legal metrology ensures transparency in measurements involved in economic transactions (Howarth *et al.*, 2008). Examples of legal metrology are found in trade of raw materials such as oil and gold where economic impact of accuracy is critical for seller and buyer.

2.1.1 Uncertainty

There is always a degree of doubt for every measurement — uncertainty of measurement (Howarth *et al.*, 2008). Consideration of measurement uncertainty is crucial for producing high-quality measurements, allowing a comprehensive understanding of results within the context of calibration, testing, tolerance specifications, etc.

There are many guides for the evaluation of the measurement uncertainty, this presentation follows the guide of Bell (2001).

There are two approaches to estimate the sources of uncertainties: ‘Type A’ and ‘Type B’ evaluations.

Type A evaluations involve uncertainty estimates by using statistical analysis, typically based on repeated readings.

Type B evaluations encompass uncertainty estimates derived from various sources, such as past measurement experiences, manufacturer's specifications, calibration certificates, published data, calculations, and common sense.

For Type A estimates of uncertainty obtained through repeated measurements, the estimated standard uncertainty, u, of the mean can be achieved from:

$$u(a) = \frac{s}{\sqrt{n}} \tag{2.1}$$

Where s is the estimated standard deviation, n represents the quantity of measurements of a within the given set.

Given the scarcity of information in certain Type B estimates, it becomes necessary to assume that the value b has an equal likelihood of occurring at any point within the range, such as a uniform or rectangular distribution. A rectangular distribution's standard uncertainty is determined as follows:

$$u(b) = \frac{w}{\sqrt{3}} \tag{2.2}$$

Where w represents the semi-range, indicating half the width separating the upper and lower bounds of b.

Standard uncertainties are combined by adding in quadrature, the result of this is shown by u_c:

$$u_c = \sqrt{u(a)^2 + u(b)^2 + \cdots etc.} \tag{2.3}$$

Where *u(a)*, *u(b)*, etc. is the standard uncertainty of each component and all the components have the same unit. If the components are corelated, we should take it into account.

In certain scenarios, it becomes necessary to express uncertainties in relative terms. For instance, when calculating the area A of a rectangular carpet by multiplying its width W by its length L (i.e. A=W x L), the relative or fractional uncertainty in the carpet's area will be determined by analysing the fractional uncertainties associated with both the width and the length.

Subsequently, the relative uncertainty u(A)/A in the area can be expressed as follows:

$$\frac{u(A)}{A} = \sqrt{\left(\frac{u(W)}{W}\right)^2 + \left(\frac{u(L)}{L}\right)^2} \tag{2.4}$$

Depending on the desired confidence interval, the combined standard uncertainty can be rescaled to a different confidence level, such as 95 percent, by employing a coverage factor, denoted as 'k'. When the combined standard uncertainty is multiplied by this coverage factor 'k', the result is termed the expanded uncertainty, symbolized by 'U':

$$U = ku_c \tag{2.5}$$

The measurement result needs to be reported together with its uncertainty. Two numbers are used to quantify an uncertainty, the interval of the result of a measurement and a confidence level. The result can be expressed:

$$Y = y \pm U, at\ a\ level\ of\ confidence\ of\ 95\% \tag{2.6}$$

Where Y is the measurand, y is the value obtained from the measurements, and U is the expanded uncertainty of that value.

2.1.2 Traceability Chain

A traceability chain, illustrated in Figure 2.1, constitutes an uninterrupted chain of comparisons, each accompanied by stated uncertainties (Howarth *et al.*, 2008). This guarantees the connection of a measurement result or standard value to references at superior levels, ultimately tracing back to the primary standard.

The calibration chain establishes a dependable understanding of measurement uncertainties by linking it to the SI definition. For instance, the cylindricity measuring machine is calibrated by using this chain. The process begins with the metre's definition, which is utilized for calibrating a laser interferometer. The calibrated interferometer is then employed to calibrate a gauge block. The gauge block is employed in the calibration of a form measuring instrument, which, in turn, is utilized to calibrate a roundness calibration standard (flick standard, see the section 3.1.2). Following that, the flick standard can be utilized to calibrate the cylindricity measuring machine. The measurement results obtained from the machine can be linked back to the

definition of the meter, as illustrated in Figure 2.1. However, it's essential to note that the uncertainty accumulates as each step further from the initial definition, leading to a proportional increase in measurement uncertainty. Additionally, as we move away from the initial standard definition, the measuring instruments become less costly but also less accurate.

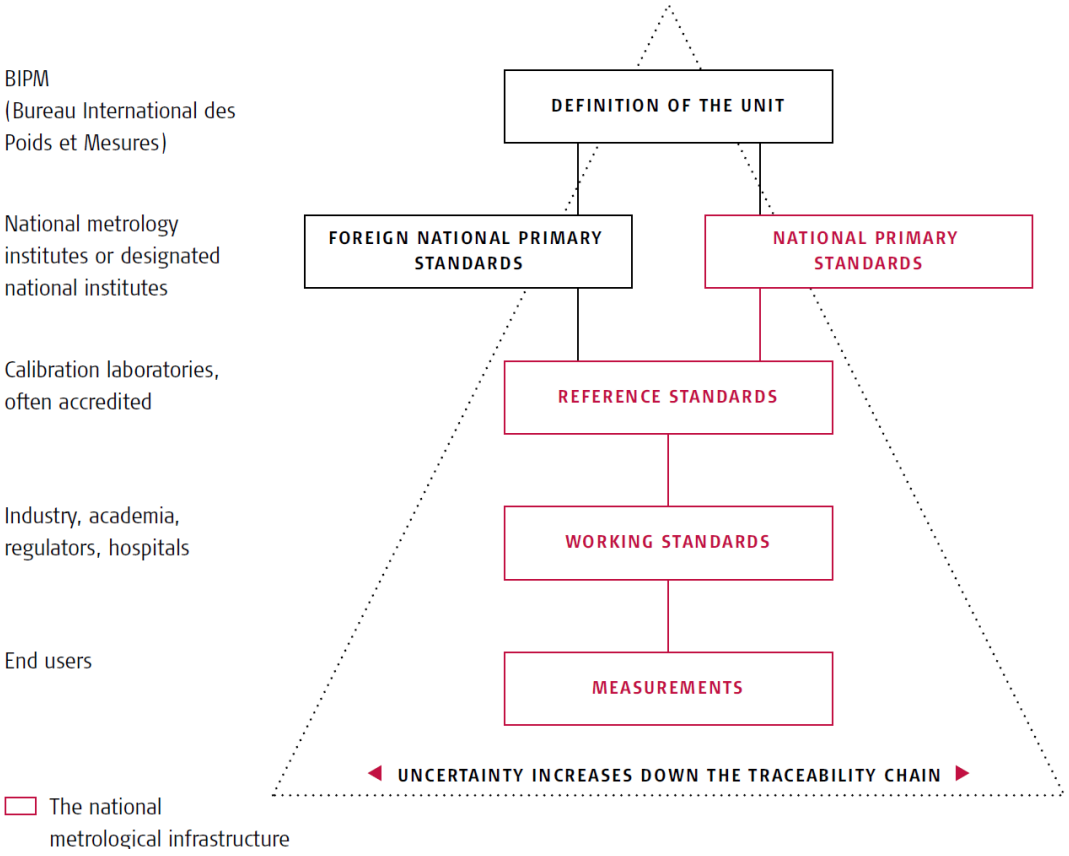

Figure 2.1: Traceability pyramid depicting a calibration hierarchy (Howarth *et al.*, 2008).

2.1.3 Calibration

Every measurement inherently involves errors, where the outcome of a measurement deviates from the actual value of the measurand. Calibration is a basic technique to identify and correct most sources of measurement error with sufficient time and resources. Calibration is the systematic process of comparing an instrument or device's measurement values against a known reference to detect and, if necessary, correct any deviations (Howarth *et al.*, 2008). Calibration can ensure the traceability of measurements, ultimately guaranteeing accuracy and reliability of the instrument in diverse applications.

2.1.4 The error sources of measurement in a calibration laboratory.

Since each measurement cannot be made under perfect conditions, inherently including errors. Measurement even in a calibration lab is subject to various error sources that can impact the accuracy of results. Factors such as the measuring device, the objective under measurement, Operator decisions, and the environment may introduce deviations in the measurement, as shown in Figure 2.2.

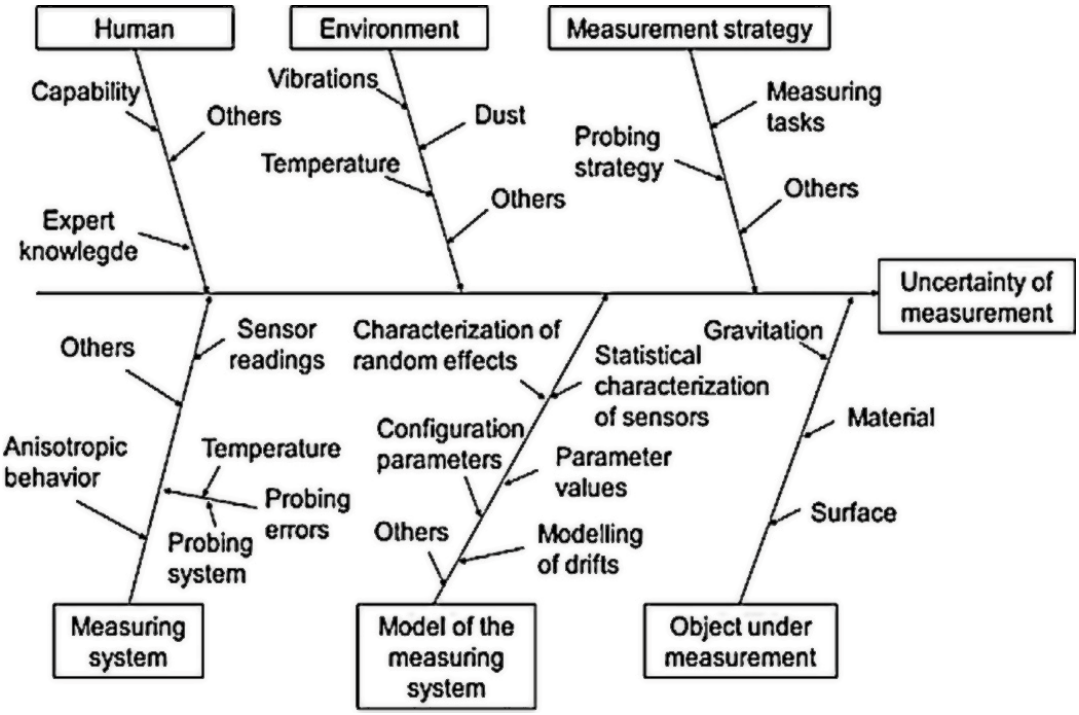

Figure 2.2: Chart of potential error sources (Schmitt *et al.*, 2016).

2.2 Cylindricity

Cylindricity is a geometric tolerance that controls the axial form, radial form, and overall shape of a cylindrical surface, ensuring that it comes close enough to a perfect cylinder in terms of roundness and straightness (Aamir, 2021). In metrology, cylindricity values plays an important role as it allows for the accurate evaluation of cylindrical forms, which are very common in industrial machining and rotating machines. The cylindricity tolerance used in technical drawings is presented in section 2.2.2. The accurate assessment of cylindricity is essential for ensuring the quality and functionality of manufactured components, thereby improving the efficiency and cost effectiveness (Lao *et al.*, 2003). The measurement of cylindricity is generally performed with roundness measuring instruments, where the tip of the stylus follows

around the cylindrical object to capture deviations from mathematically ideal cylinders, as shown in Figure 2.3.

Figure 2.3: A cylindricity measuring instrument (Roundtest RA-2200AH, 2024).

2.2.1 Calibration of cylindricity measuring equipment

The calibration of cylindricity measuring equipment in this thesis is carried out by using flick standard, glass hemisphere standard, and cylinder standard. The glass hemisphere standard, generally made of glass, is used for testing the spindle of the instrument, as shown in Figure 2.4. The imperfections in the shape of this sphere are usually less than 30 nm. To assess the quality of vertical linear guidance, a standard cylinder is employed (see Figure 2.4), and its shape imperfection is typically under 400 nm (Vissiere *et al.*, 2013).

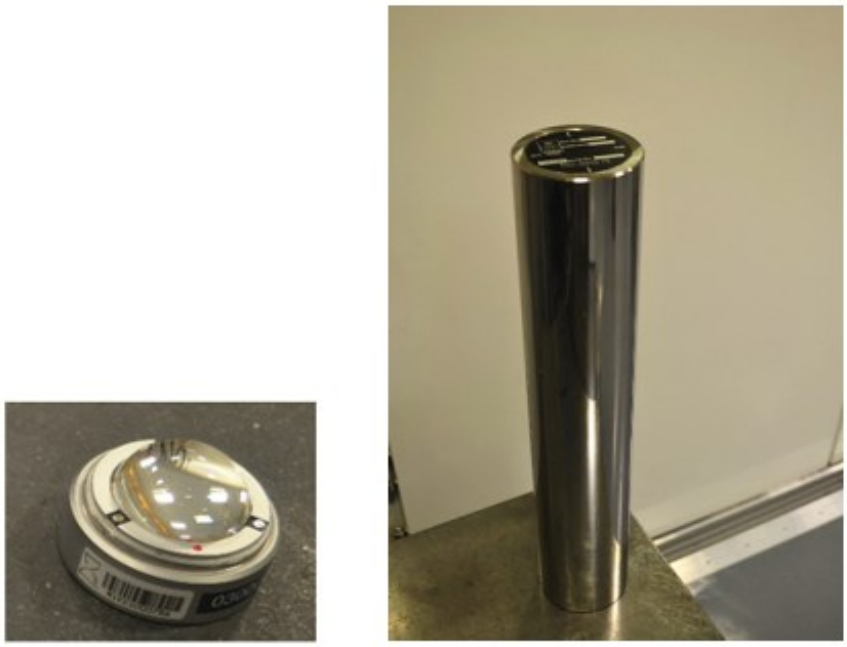

Figure 2.4: Glass hemisphere standard and cylinder standard.

2.2.2 Cylindricity tolerance

In technical drawings, the cylindricity tolerance is described as the acceptable degree of variation from the ideal cylindrical shape for a given feature. It outlines the permissible range within which the actual cylindricity of the feature can vary according to GPS (Geometrical Product Specification) standards defined in the ISO 1101 standard, as shown in Table 1.

Table 1: Cylindricity tolerance (SFS-EN ISO 1101, 2006).

Symbol	Definition of the tolerance zone	Indication and explanation
⌭	18.4 Cylindricity tolerance (see ISO/TS 127801 and ISO/TS 127802)	
	The tolerance zone is limited by two coaxial cylinders with a difference in radii of *t*. 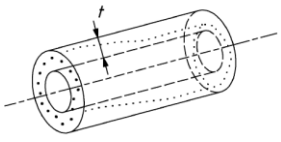	The extracted (actual) cylindrical surface shall be contained between two coaxial cylinders with a difference in radii of 0.1. 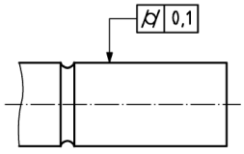

The standard defines that the tolerance zone is determined by two coaxial cylinders with a defined difference in radii (t), serving as a critical parameter in assessing conformity. This tolerance ensures that the actual cylindrical surface resides within the boundaries of two coaxial cylinders, maintaining a specific difference in radii.

2.2.3 Defects Identification

To establish the concept of cylindricity in more detail, the standard ISO 12181-1:2011 is utilized to defines the roundness parameters. We will also reference the standards ISO 12180-1:2011 and ISO 12180-2:2011. ISO 12180-1, titled “Part 1: Vocabulary and parameters of cylindrical form,” defines the terminology and ideas associated solely with the cylindricity of individual complete integral features. Additionally, ISO 12180-2, titled ‘Part 2: Specification operators,’ further clarifies the complete specification operator for the cylindricity of only complete integral features, specifically addressing the geometrical properties associated with the cylinder type’s features.

Roundness is a property of a circle, measuring how closely the shape of an object approaches a perfect circle (ISO 12181-1, 2011). It assesses the deviation of the object's surface from an ideal circular form, ensuring uniformity in all radial directions (ISO 12180-1, 2011).

Two types of perfect circle will be included in this thesis, least squares reference circle (LSCI) and minimum zone reference circles (MZCI). By minimizing the sum of the squares of the radial deviations from the circle, the LSCI provides an optimal representation of the profile's geometric centre (Figure 2.5). This approach is widely utilized in precision engineering to assess and enhance the roundness of components. However, MZCI consists of two concentric circles that just enclose a given profile with the smallest possible radial separation. The centre point of these circles is called the minimum zone centre (Figure 2.6).

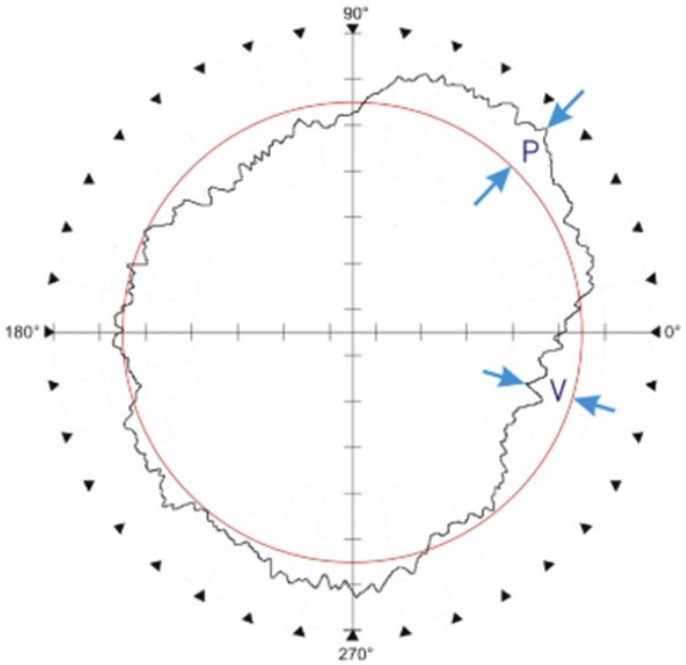

Figure 2.5: Least squares reference circle (LSCI), RONt = distance P + V (Exploring Roundness A fundamental guide to the measurement of cylindrical form, no date).

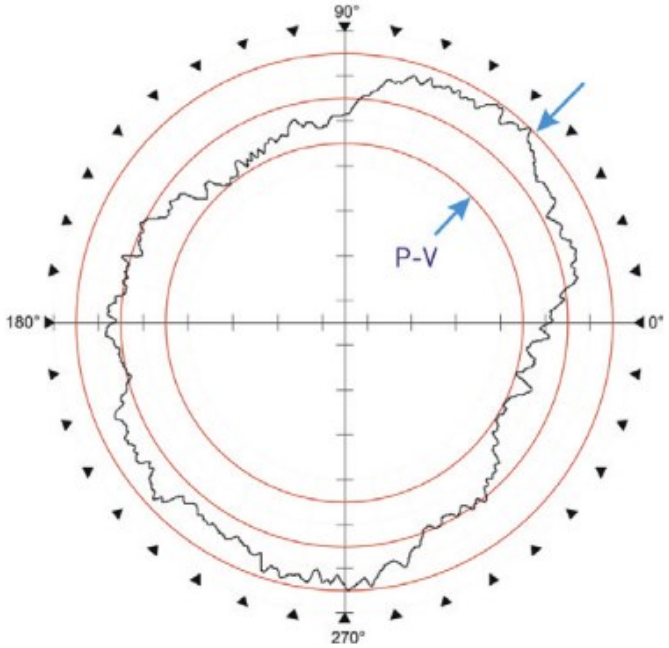

Figure 2.6: Minimum Zone reference circle (MZCI), RONt = distance P – V (Exploring Roundness A fundamental guide to the measurement of cylindrical form, no date).

The parameter Roundness Total (RONt) is referred as peak-to-valley roundness deviation according to the standard ISO 12181-1:2011. It is the most used parameter. RONt is defines as the separation of two circles concentric with the centre of the reference circle that just enclose the data. For the least squares reference circle, the RONt is defined by the maximum deviation of the profile from the LSCI, measured from the highest peak to the lowest valley, as shown in Figure 2.5. However, for the minimum zone reference circle, the RONt is given as the radial separation of the two circles, as described in Figure 2.6.

The reference cylinder is defined as the "associated cylinder fitting according to specified conventions to the cylindricity surface" (ISO 12180-1, 2011). The term "specified conventions" designated the method of extracting the reference cylinder from the cylindricity surface. The least squares method creates a least squares cylinder using roundness planes measured at different heights. It finds a best fit line, called the least squares axis, through the centres of these planes. The least squares reference cylinder is made by analysing the radial departures of all the measured data from this axis, see Figure 2.7.

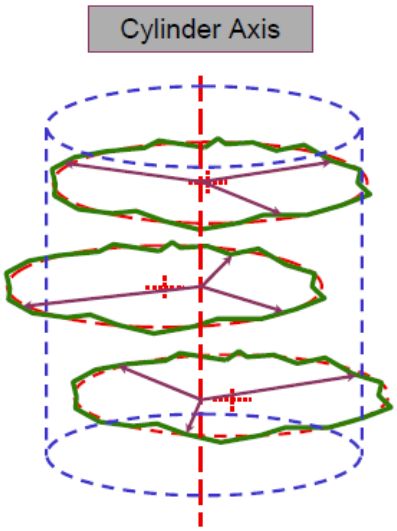

Figure 2.7: Least squares reference cylinder (LSCY).

On the other hand, the minimum zone cylinder is another geometric concept that focuses on minimizing the radial distance between two cylinders that envelop the measured data points. The cylindricity deviation from peak to valley is defined with respect to minimum zone reference cylinders. It is determined by summing the magnitude of the maximum positive local cylindricity deviation with the absolute value of the maximum negative local cylindricity deviation, as shown in Figure 2.8.

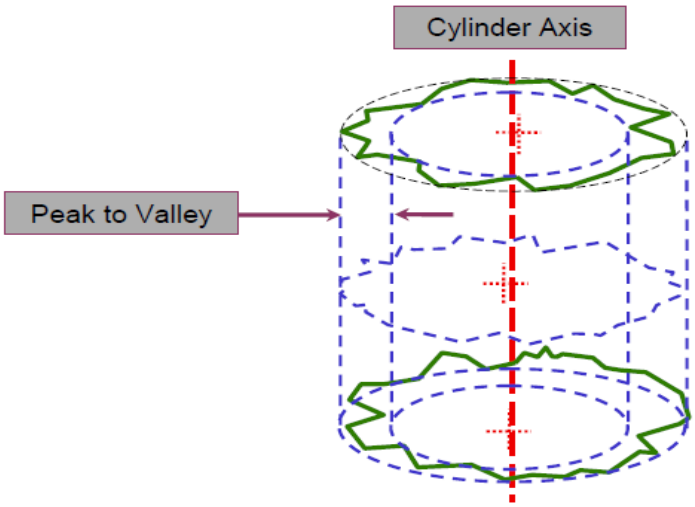

Figure 2.8: Minimum zone reference cylinder (MZCY).

The reference cylinder helps establish the concept of cylindricity deviation. The cylindricity deviations from cylindrical shape are measured with respect to this reference cylinder (ISO 12180-1, 2011). Figure 2.9 shows the concept of local cylindricity deviation, which refers to the perpendicular deviation from the reference cylinder to a point on the cylindricity surface.

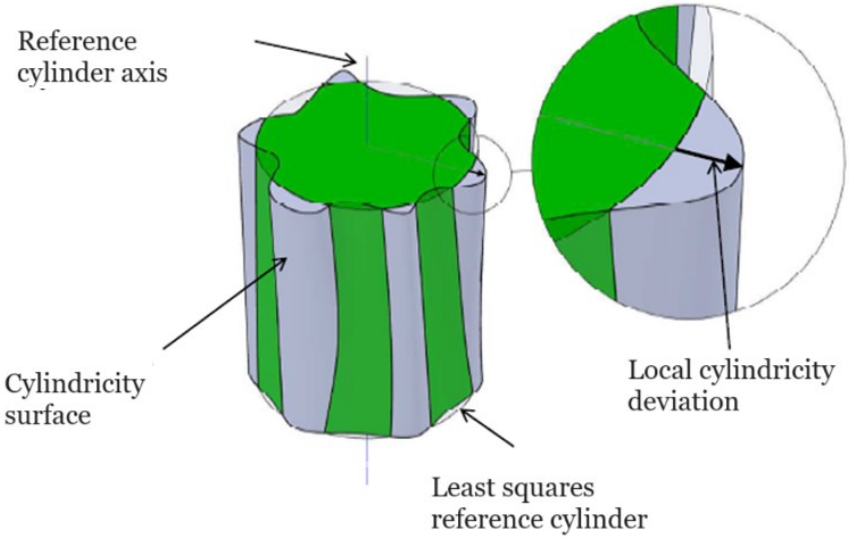

Figure 2.9: Definitions from the ISO 12180-1 standard.

Cylindricity deviation encompasses three distinct forms: median line deviations, radial deviations, and cross-section deviations, as described in Figure 2.10. The median line deviation involves the straightness of the median line. Radial deviation can be defined through the evaluation of the generatrix profile's parallelism to the cylinder axis, taken as a datum line. Additionally, cross-section deviations are characterized by the roundness of the cross-

sectional profiles. In practice, the observed deviation is a combination of these three types of cylindricity deviation (Zhao, Zhang and Zheng, 2010).

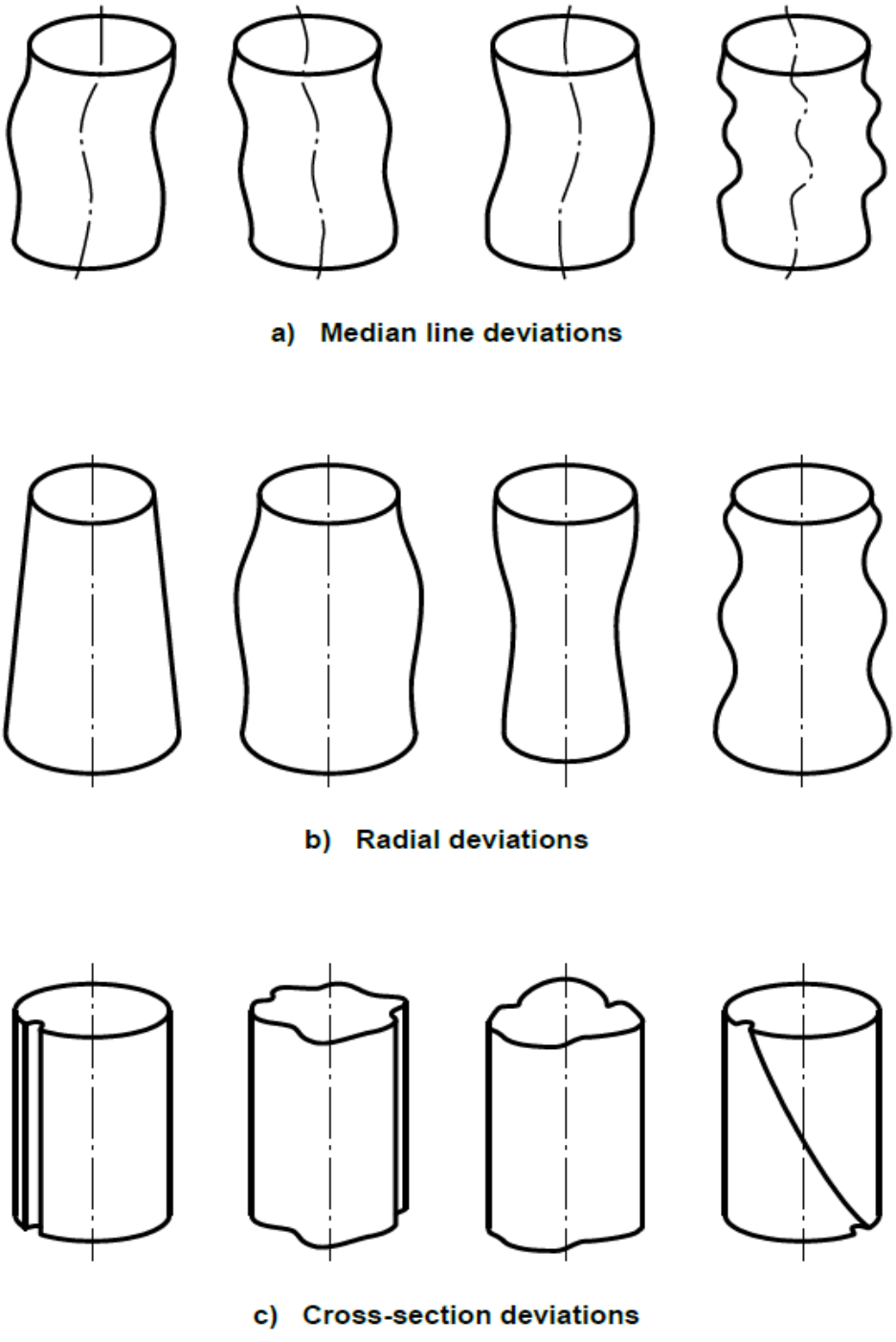

Figure 2.10: Deviations from cylindrical form (ISO 12180-1, 2011).

2.2.4 Cylindricity Measuring Instrument

Figure 2.11 describes the architecture of cylindricity measuring instrument. It is consisted of the base, the rotary worktable, the vertical and horizontal movement, and the stylus. The workpiece is placed on the rotary worktable, which is attached to the rotational air bearing generating precise rotational movement. The vertical column guides the movement of the carriage featuring a horizontal arm structure. During the workpiece rotation, a probe which is attached to the arm's end detects the deviation of surface position. These instruments are not intended for accurate measurement of diameter.

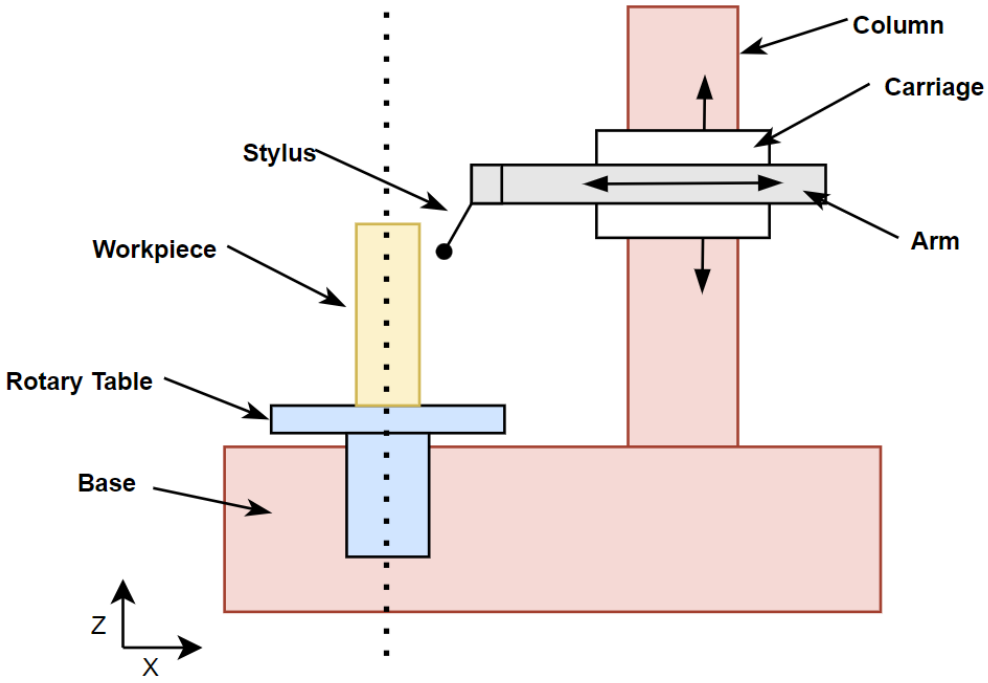

Figure 2.11: The diagram of a traditional cylindricity measuring instrument vertical movement along column and the horizontal movement along the arm.

Figure 2.12 shows three principal sources of error for the cylindricity measuring machine, including the spindle's spatial rotation deviation, the error in the straight guide's straight motion, and the error of parallelism between the spindle and the guide. To enhance the cylindricity measuring machine's measuring precision, these errors sources should be reduced or eliminated. However, it is challenging to separate these errors from the cylindricity measurement in high accuracy cylindricity measurement. To overcome the problem, the reversal method for cylindricity compound errors is designed and applied to the cylindricity measuring to enable the separation of cylindricity compound error totally (Xue and Ye, 2006). This method is created by utilizing the fact that movement errors at the cylindrical object's two radial ends

always move in opposite directions. It separates the cylindrical surface shape through a combination of sensors, an error separation table, and adding measured signals from different positions.

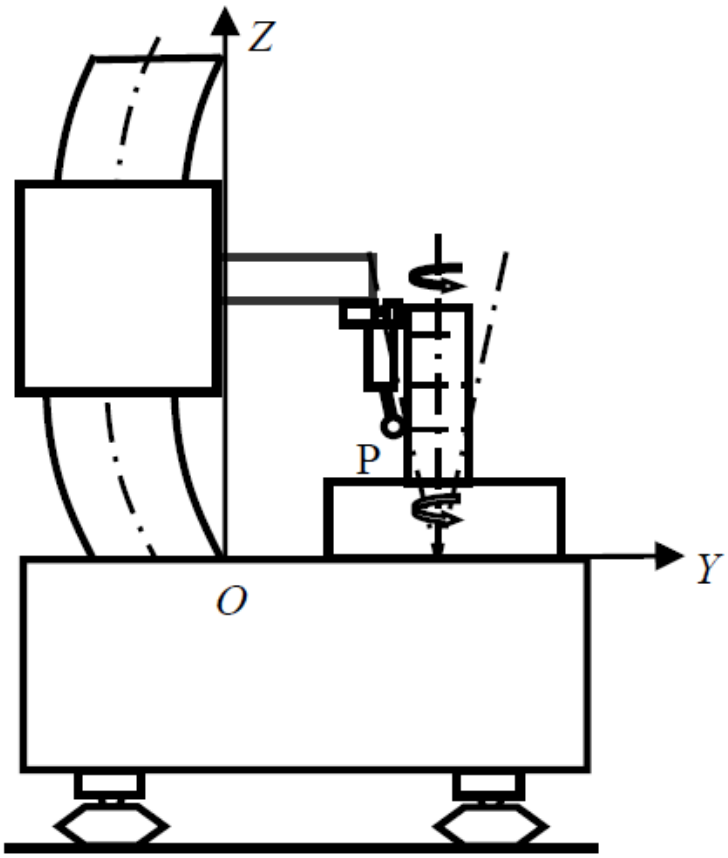

Figure 2.12: Schematic diagram of the effect of error sources when measuring cylindricity.

Figure 2.13 illustrates key features of a roundness system, showcasing various movements and associated defects found in traditional cylindricity measuring machines. The aerostatic spindle exhibits run-out (7) and radial defects (5 & 6), while vertical and horizontal translations reveal a lack of straightness (2) and (3). Additionally, uncertainties impact parallelism (1) between the spindle rotation axis and the axis of vertical translation. as well as perpendicular (4) between the horizontal translation axis and the spindle rotation axis.

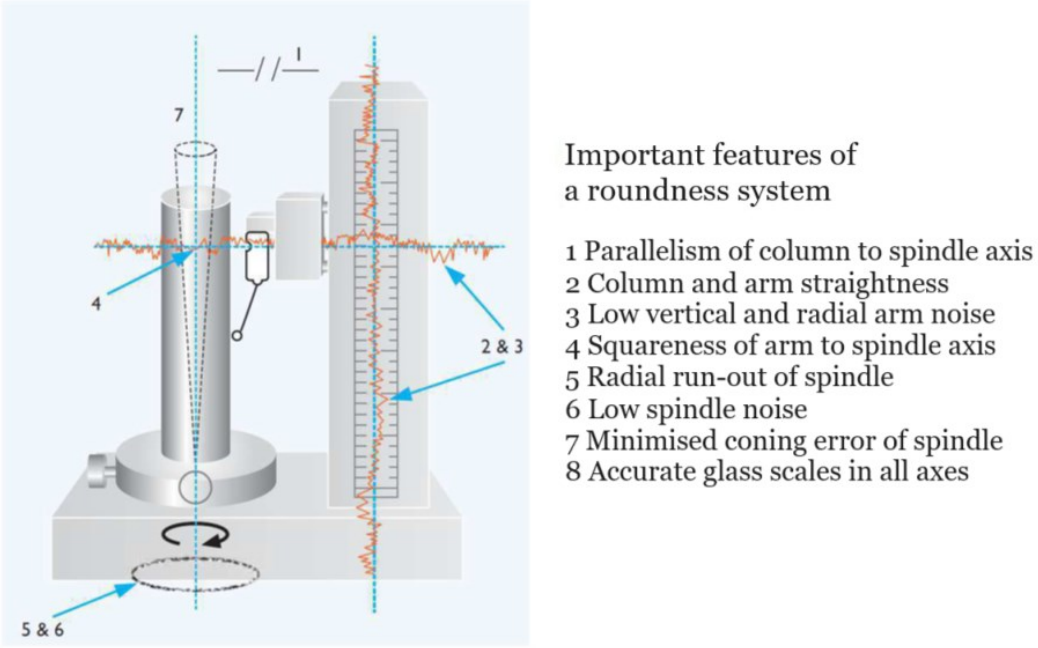

Figure 2.13: Error sources of conventional cylindricity measuring instrument (Vissiere *et al*., 2013).

Cylindricity measurement combines straightness and circularity measurements. Consequently, the uncertainty in a cylindricity measurement reflects the combined uncertainties related to the probe, part rotation, probe's vertical translation, and the parallelism between the translation and rotation. Each of faults impacts the measurements result uniquely. Figure 2.14 illustrates the influence of each fault on the cylindricity measurement outcome.

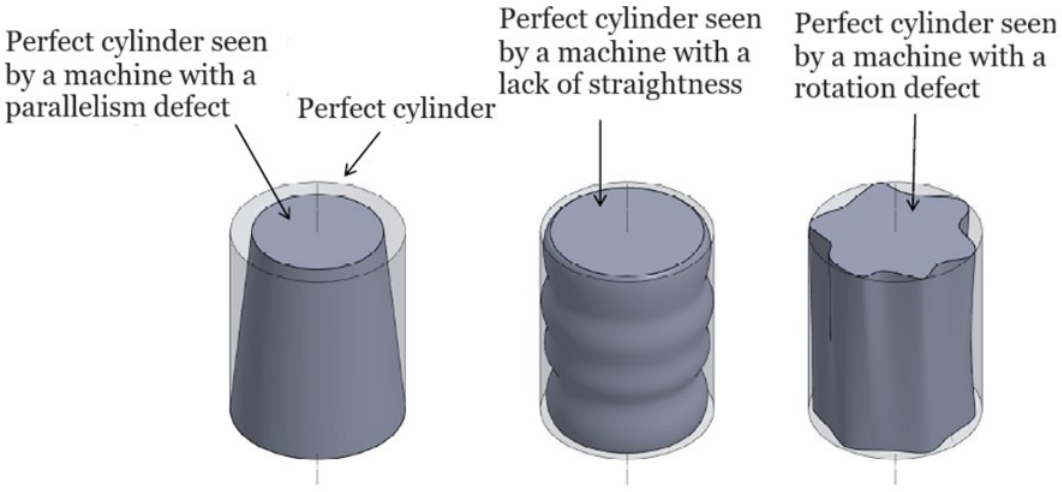

Figure 2.14: Link between machine faults and measurement errors (Vissiere *et al*., 2013).

2.2.5 Error separation methods

Many error separation methods have been developed, aiming to improve accuracy. The reversal method involves taking two measurements with a 180-degree rotation of both the artifact and displacement indicator to differentiate between spindle error and artifact out-of-roundness (Marsh, Arneson and Martin, 2010). While considered superior due to its theoretically perfect separation, it requires meticulous hardware design and synchronization. A rotary table-based method was proposed to streamline meeting these geometric requirements (Marsh, Arneson and Martin, 2010).

On the other hand, the multi-probe method involves simultaneous measurements from multiple position sensors to distinguish spindle error from artifact out-of-roundness (Grejda, Marsh and Vallance, 2005). This method does not require the synchronous error's calculation before implementation, unlike the reversal method. Additionally, it offers advantages in situations where accurate indexing of the artifact and sensors during evaluation is inconvenient or impossible.

Since traditional multi-step methods face challenges with harmonics suppression, two-step method utilizes Prony spectrum analysis and singular value decomposition to further improve in accuracy and simplify the measuring procedure (Sun, 1996). This approach allows for the identification and analysis of harmonic components in the data series, leading to improved precision in roundness measurements.

The Full-harmonic error separation technique offers a precise method for separating systematic spindle errors and roundness errors of workpieces (Cao *et al.*, 1992). By employing equi-angular indexing and digital filtering, the technique can enhance measurement accuracy from nanometre to sub-nanometre levels. It efficiently separates harmonic errors within 1-500 undulations per revolution (UPR), reducing the need for high indexing accuracy of the turntable.

3 Research material and methods

3.1 Equipment

3.1.1 Taylor Hobson cylindricity measuring machine

The Taylor Hobson cylindricity measuring machine Talyrond 262 was used in the thesis, the detailed specifications are summarized in the Table 2. The instrument is over 20 years old and previous calibrations have shown that it does not fulfil all specifications in Table 2. However, its accuracy is believed to still fulfil the needs of VTT MIKES and requirements of its customers.

Table 2: Specifications of errors (Data_Sheet_Talyrond262, 2024).

Measurement Capacity	
Maximum Diameter	350 mm
Maximum Weight	50 Kg
Maximum Height	500 mm
Worktable & Spindle	
Worktable Diameter	260 mm
Speed of Rotation	6 rpm and 2 rpm nominal, clockwise
Range of Centring	5 mm
Range of Levelling	1 degree
Roundness Limit of Error (Departure from Least Squares Circle at 6 rpm with 0-50 u.p.r filter)	Concentric Load within 0.04 μm + 0.0003 um/mm height above worktable
Axial Error	0.06 μm maximum axial movement of worktable during one resolution
Vertical Straightness Module	
Measurement Length	500 mm
Straightness Limit of Error (Minimum Zone Straightness at 5 mm/sec with 8.0 mm cut-off low pass filter	1.5 μm over 500 mm and 0.25 μm over any 100 mm traverse length
Positional Control Uncertainty	± 100μm for one single move
Motorised Radial Arm	
Straightness Accuracy	0.5 μm over 200 mm and 0.25 μm over any 50 mm traverse length
Traverse Length	200 mm. This may be set for up to 50 mm of travel past the spindle axis
Positional Control Uncertainty	± 50μm for one single move
Gauge	
Standard Stylus Arm Length	100 mm
Range of Gage Movement with 100 mm Stylus Arm	2.0 mm Nominal

3.1.2 Reference pieces

Table 3 summarises the information of the reference pieces in the laboratory which are used in this thesis. The Flick standard is a cylindrical artifact utilized for the calibration and verification of cylindricity measuring instruments. It consists of a precisely manufactured cylinder with accurately controlled dimensions and surface characteristics, as shown in Figure 3.1 (Kumar *et al.*, 2022). In this thesis, the flick standards with nominal depths of 2.55 μm, 12.20 μm, and 23.10 μm were used.

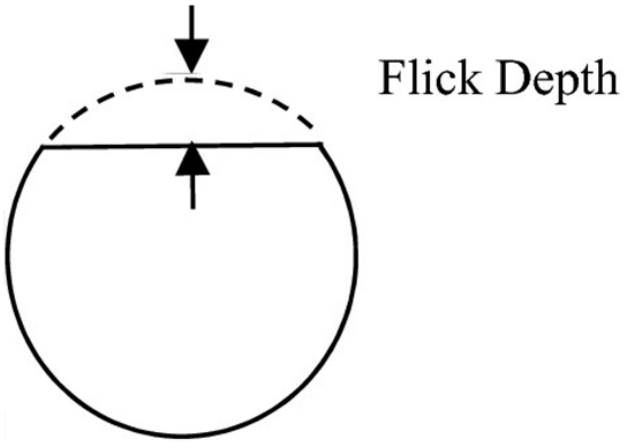

Figure 3.1: The flick standard schematic diagram.

Conversely, the glass hemisphere standard is another commonly employed reference tool for assessing roundness, featuring a glass sphere with extremely high precision in terms of roundness.

The cylinder standard serves as a fundamental reference for assessing cylindricity in metrology. It comprises a precisely crafted cylindrical steel object with known geometric properties, such as diameter and roundness. Metrology laboratories utilize this standard to calibrate and validate their capability to measure cylindricity accurately, especially the straight guide's straight movement and parallelism between the spindle and column axes.

The straightness standard is a precision instrument designed for the inspection of straightness of various types of equipment, such as machine tools and form measurement machines. The straightness standard at VTT MIKES is a 700 mm long piece with a dimension of 740 mm x 35 mm x 50 mm. It is made of alumina ceramic which can enable high resistance to abrasion and little secular change. The straightness deviation is 0.2 μm according to the calibration certificate.

Table 3: The information of the reference pieces in the laboratory.

Reference Standard	Name	Code No.	VTT MIKES No.
	2.55 µm Flick standard	112/434-155	MIKES000784
	12.20 µm Flick standard	112/435-168	MIKES000785
	23.10 µm Flick standard	112/2308-3957	MIKES000824
	Glass hemisphere standard	112/436-875F	MIKES000786
	Cylinder standard	112/1997-R526	MIKES000934
	Ceramic Straight-ness standard	311-335-22	MIKES009052

3.2 Measurement

Before conducting measurements using a cylindricity measuring machine, centring, as outlined in Appendix A, is an important step. The measurement accuracy greatly depends on this step, emphasizing the need for thorough

understanding and adherence to the provided guidelines. Furthermore, to mitigate potential inaccuracies, it is recommended to allow the machine to run for at least 30 minutes upon activation, allowing it to stabilize and achieve optimal operating conditions.

3.2.1 Evaluation of radial error of rotary table by error separation for Talyrond

The measurements were conducted after the centring process. The measurements of roundness on the glass hemisphere were conducted to evaluate the radial error of rotary table. During the measurements, the multi-step four-position error separation method was applied, where only the part is rotated, not the probe. Figure 3.2 illustrates the orientations of the part and probe in the four positions. This method can separate and eliminate the systematic portion of the radial error in the rotary table from the collected data. For example, if a bump appears in the same position on the curve when the glass hemisphere is shifted to positions b, c, and d, it indicates that the error originates from the rotary table. However, if the bump moves along the shifted position, the error is attributed to the glass hemisphere (Muralikrishnan and Raja, 2009).

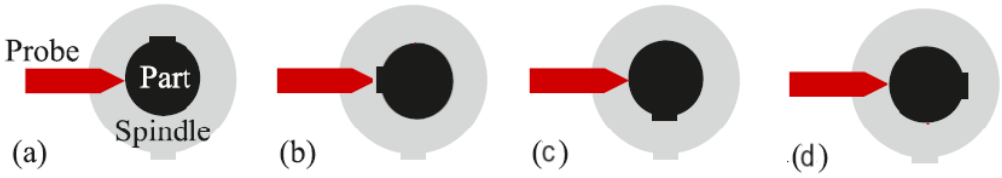

Figure 3.2: Position a. Position b. Position c. Position d. A *rectangular key* is shown in both the part and the spindle to indicate relative angular positions at the start of each measurement.

Figure 3.3 demonstrates a measurement in which the stylus is measuring the roundness of the glass hemisphere standard using four-position method. The four-position error separation method consists of four steps.

- Fix the glass hemisphere standard on the chuck properly.
- Position the stylus to the first position (Position a) to measure the roundness at the height of approximately 75 mm above the rotary worktable.
- Conduct the roundness measurement function of the Talyrond cylindricity measuring instrument five times and record the data.
- Repeat the roundness measurement for Positions b, c, and d, by rotating the part to each new position.

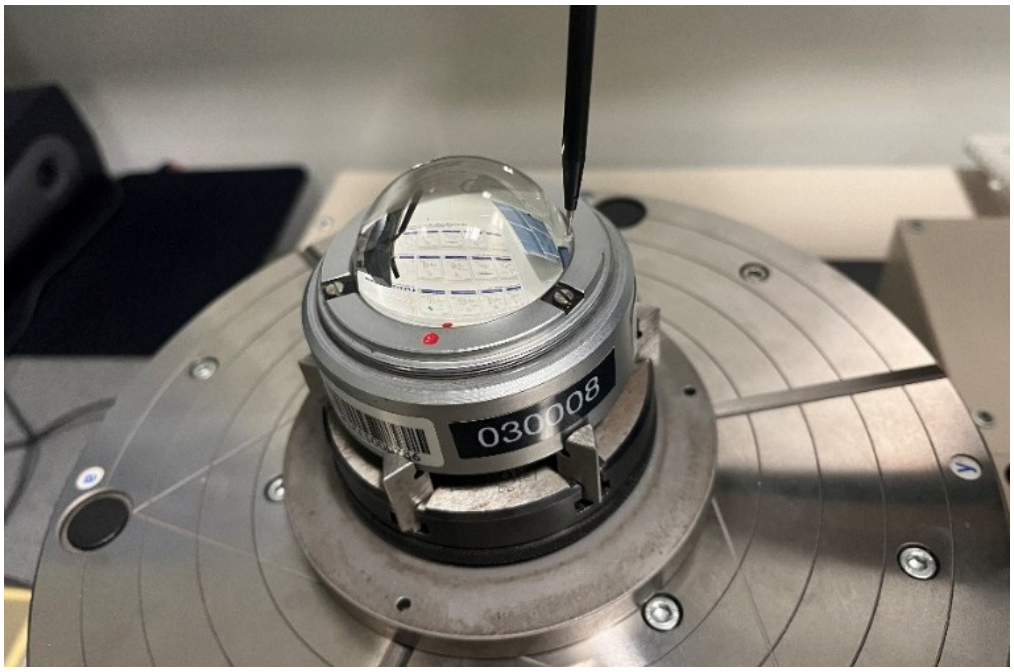

Figure 3.3: Demonstration of the roundness measurement in which the stylus is measuring the glass hemisphere standard's roundness.

A representative measurement outcome depicting the roundness of the glass hemisphere standard, RONt, is 0.12 µm, as illustrated in Figure 3.4.

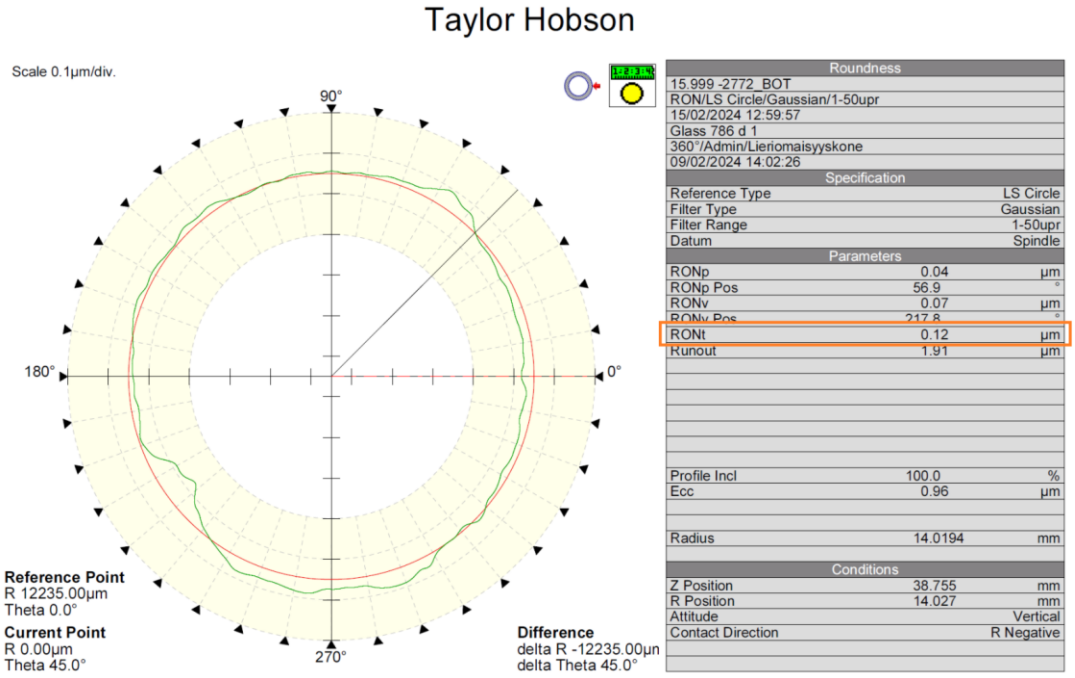

Figure 3.4: The roundness of the glass hemisphere standard in a typical measurement is 0.12 µm, using a Gaussian filter with a range of 1-50 UPR.

The measurement data set was then analysed by using MATLAB script, detailed in Appendix B. Firstly, the averages for positions a, b, c, and d (vectors *avga*, *avgb*, *avgc*, *avgd*) were computed to ensure the accuracy and reliability of the results.

In theory, calculating the average for a data set helps to separate error sources and emphasize the contributions of the elements we are interested in. The next step is to calculate the mean of the averages obtained from each position, denoted as vector *RTe*, which can represent the radial error of the rotary table from the collected roundness data.

According to the definition of the RONt mentioned in section 2.2.3, the evaluated radial error of the rotary table, vector *RTee*, was determined by subtracting the maximum value of the *RTe* from its minimum value. The results of the MATLAB script are depicted in Figure 3.5. The evaluated radial error of the rotary table, *RTee*, is 48 nm.

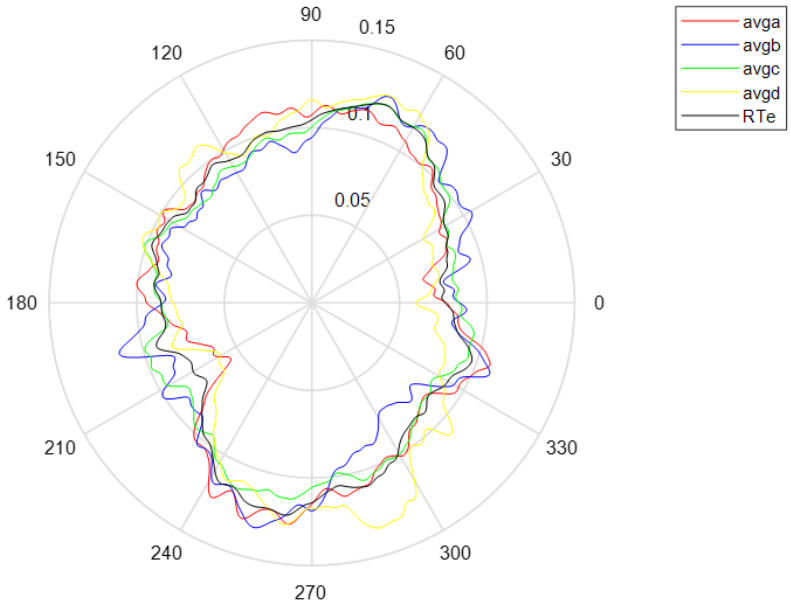

Figure 3.5: Evaluated radial error of the rotary table, which is 48 nm. The unit for radial axis is μm.

Similarly, the measured roundness data for positions b, c, and d were shifted by 90°, 180°, and 270° counterclockwise, denoted as vectors *shiftedavgb*, *shiftedavgc*, and *shiftedavgd*. Next, taking the average for the *avga, shiftedavgb*, *shiftedavgc*, and *shiftedavgd* can average out the radial error of the rotary table and remain the roundness error of the glass hemisphere *(*vector *Ge)*. Finally, the evaluated roundness error of the glass hemisphere, vector *Gee*, was determined by subtracting the maximum value of the *Ge* from

its minimum value. Figure 3.6 illustrated that the evaluated glass hemisphere's roundness error is 33 nm, which is smaller comparing with Figure 3.4 because of the error separation and averaging.

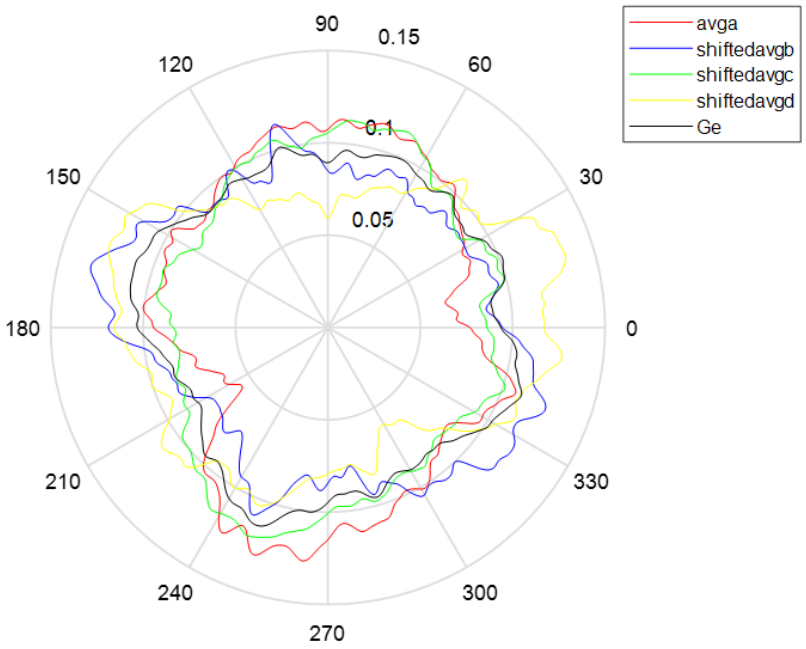

Figure 3.6: The evaluated glass hemisphere's roundness error is 33 nm, using error separation method. The unit for radial axis is μm.

3.2.2 Evaluation of axial error of rotary table by for Talyrond

The measurement of flatness on the glass hemisphere standard can be performed to detect the axial error of rotary table. Figure 3.7 shows the measurement in which the stylus is tracking the vertical movement of the glass hemisphere standard. The measurement process is divided into four steps.

- Secure the glass hemisphere standard on the chuck.
- Position horizontally the stylus.
- Adjust the stylus at the top centre of the glass hemisphere standard.
- Conduct the flatness measurement function of the Talyrond cylindricity measuring instrument five times and record the data.

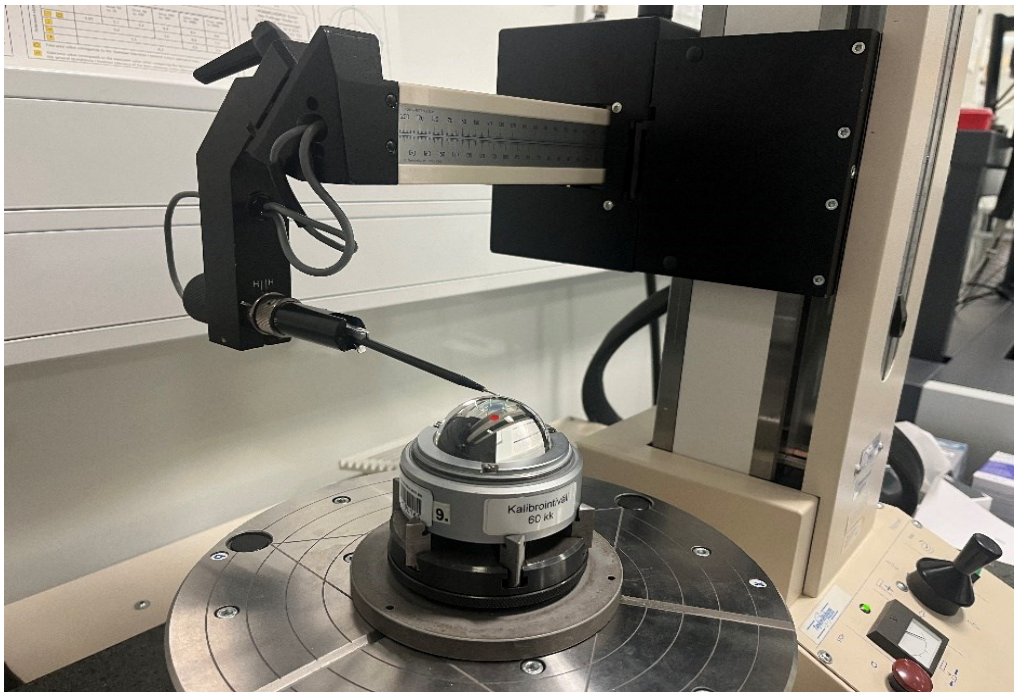

Figure 3.7: The probe is measuring the axial error of the rotary table.

A typical measurement result of the of glass hemisphere standard's flatness, FLTt, is 30 nm, as shown in the Figure 3.8.

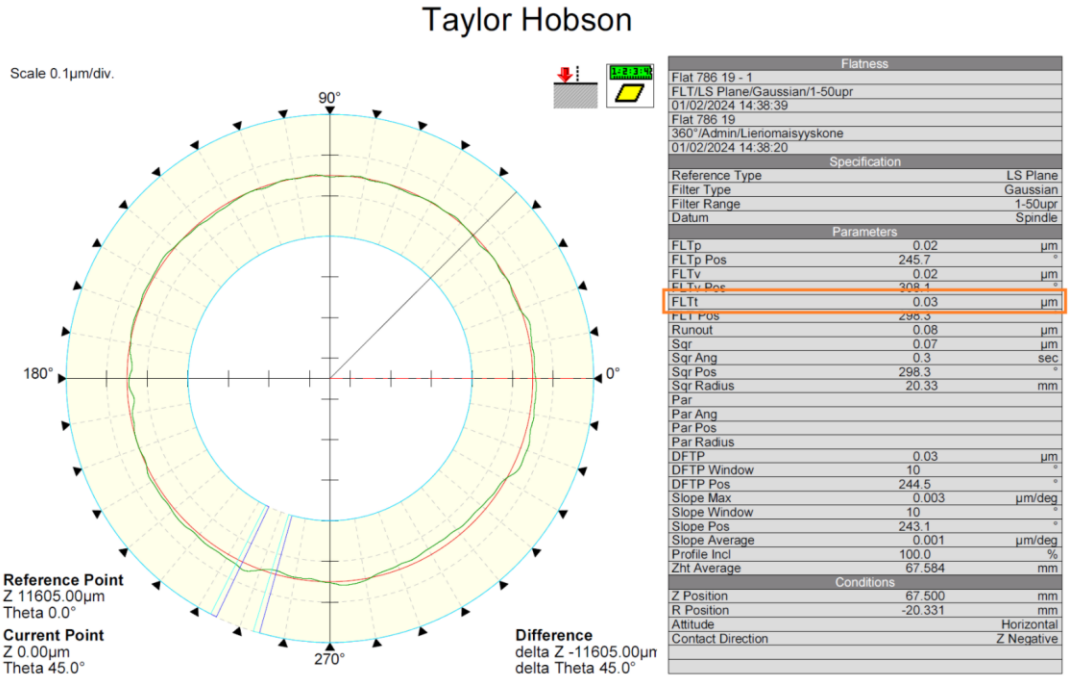

Figure 3.8: A typical measurement result of the glass hemisphere standard's flatness, FLTt, is 30 nm, using a Gaussian filter with a range of 1-50 UPR.

3.2.3 Evaluation of the precision of the probe for Talyrond

The error observed in the roundness results of the flick standards may be attributed partly to the rotary table but predominantly to the probe. Therefore, the error of the probe can be separated by measuring the roundness of the flick standards with nominal depths of 2.55 µm, 12.20 µm, and 23.10 µm. Figure 3.9 shows the probe measuring the roundness of the flick standard. Furthermore, the angle of the stylus during measurement is critical; an excessively large angle may hinder measurement of inner surfaces. In our scenario, 5° represents the optimal angle for accurate measurement.

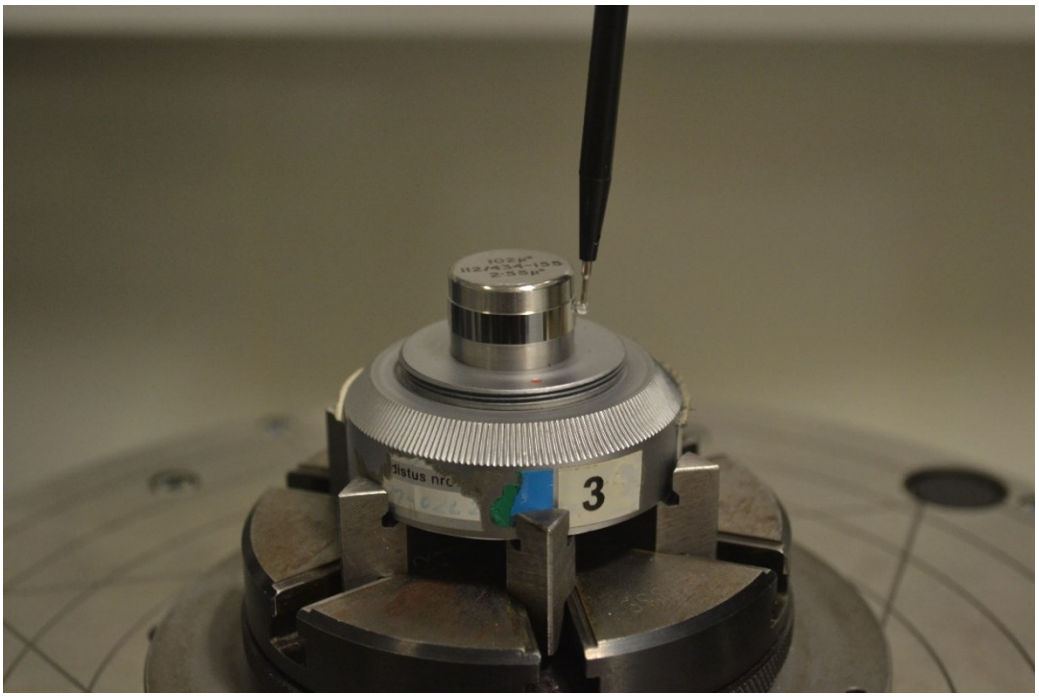

Figure 3.9: The probe is measuring the roundness of the flick standard to evaluate the precision of the probe.

After setting the angle to 5°, determining a correction factor becomes crucial to enhance the accuracy of the cylindricity measuring machine. To optimize this factor, multiple rounds of measurements on flick standards with nominal depths of 2.55 µm, 12.20 µm, and 23.10 µm were conducted using varying correction factors.

Table 4 presents the measurements obtained when the correction factor was set to 1.1007139, resulting in RONt values of 2.85 µm, 12.8 µm, and 23.57 µm, which were slightly larger than desired.

Table 4: The results of measurements when the correction factor is 1.1007139.

Flick Standard	Reference value from calibration 2020	Measurement result			Average	Deviation 2024 (µm)	Deviation 2024 (%)
112/434-155	2.72	2.99	2.78	2.77	2.85	0.13	4.45
112/435-169	12.35	12.8	12.8	12.8	12.80	0.45	3.52
112/2308-3957	23.42	24.77	22.9	23.04	23.57	0.15	0.64
						Average	2.70

In subsequent trials, the measurements were repeated with a correction factor of 1.07. Table 5 shows the measurements results, indicating RONt values of 2.66 µm, 12.41 µm, and 24.11 µm, which meet the accuracy requirements.

Table 5: The results of measurements when the correction factor is 1.07.

Flick Standard	Reference value from calibration 2020	Measurement result			Average	Deviation 2024 (µm)	Deviation 2024 (%)
112/434-155	2.72	2.64	2.67	2.66	2.66	-0.06	-2.38
112/435-169	12.35	12.41	12.41	12.42	12.41	0.06	0.51
112/2308-3957	23.42	23.97	24.21	24.15	24.11	0.69	2.86
						Average	0.33

3.2.4 Evaluation of the parallelism error between the spindle axis and column using error separation method for Talyrond.

Currently, a common technique for separating cylindricity errors is the upside-down approach. As illustrated in Figure 3.10, the upside-down method aims to reduce the straight guide's inclination to the rotating spindle throughout the height of the cylinder (positions 0 and N in figure 3.10). This inclination serves as an estimate of the parallelism between the spindle and the vertical straight guide (Xue and Ye, 2006).

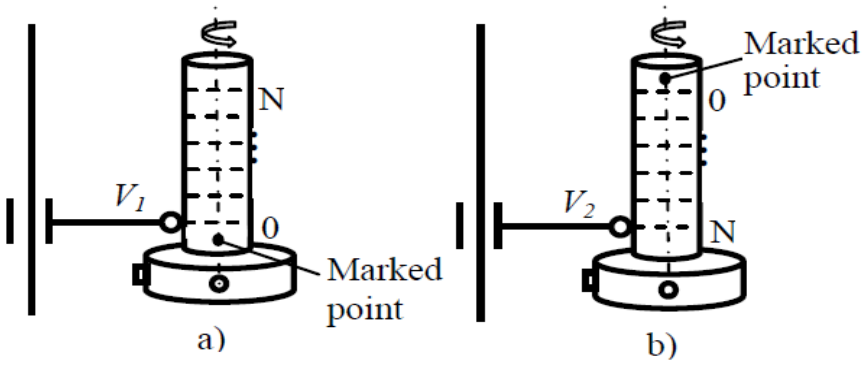

Figure 3.10: Upside-down method with single sensor (Xue and Ye, 2006).

Figure 3.11 shows the cylindricity measuring instrument is measuring the cylindricity of the cylinder standard in the calibration laboratory. The upside-down method involves four steps.

- The upright cylinder standard is assessed at 3,600 sampling points per section at 21 circular sections along a length of 23.9 mm.
- Then, the upside-down cylinder standard is measured in the same way.
- The straight guide's inclination to the rotating spindle can be achieved for both the upright cylinder standard and the upside-down cylinder by using a MATLAB script.
- The parallelism error between the spindle and the vertical straight guide can be separated from the measured cylindricity error (CYLt) by calculating the average of these two inclinations.

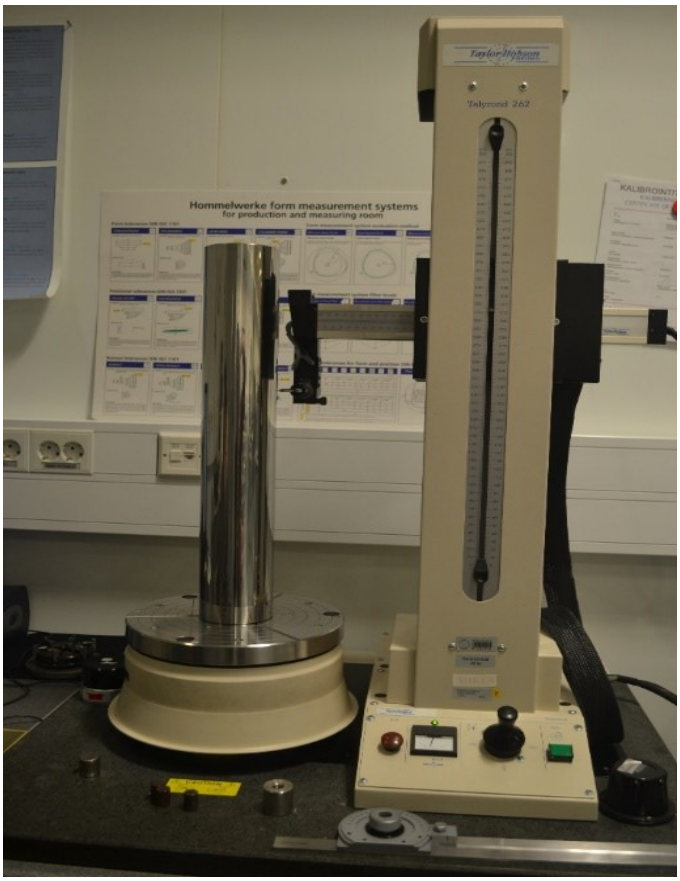

Figure 3.11: The probe is measuring the cylindricity of the cylinder standard.

A typical measurement result of the cylindricity of the cylinder standard is illustrated in Figure 3.12, its cylindricity, measured using a Gaussian filter with a range of 1-150 UPR, is 6.59 μm. It is also observed that the shape resembles a conical shape, suggesting the presence of parallelism errors in the cylindricity measuring instrument. Noticeably, recent years of experience

have typically shown a conical shape in most measurements, which could indicate a parallelism error between the spindle and the vertical guide.

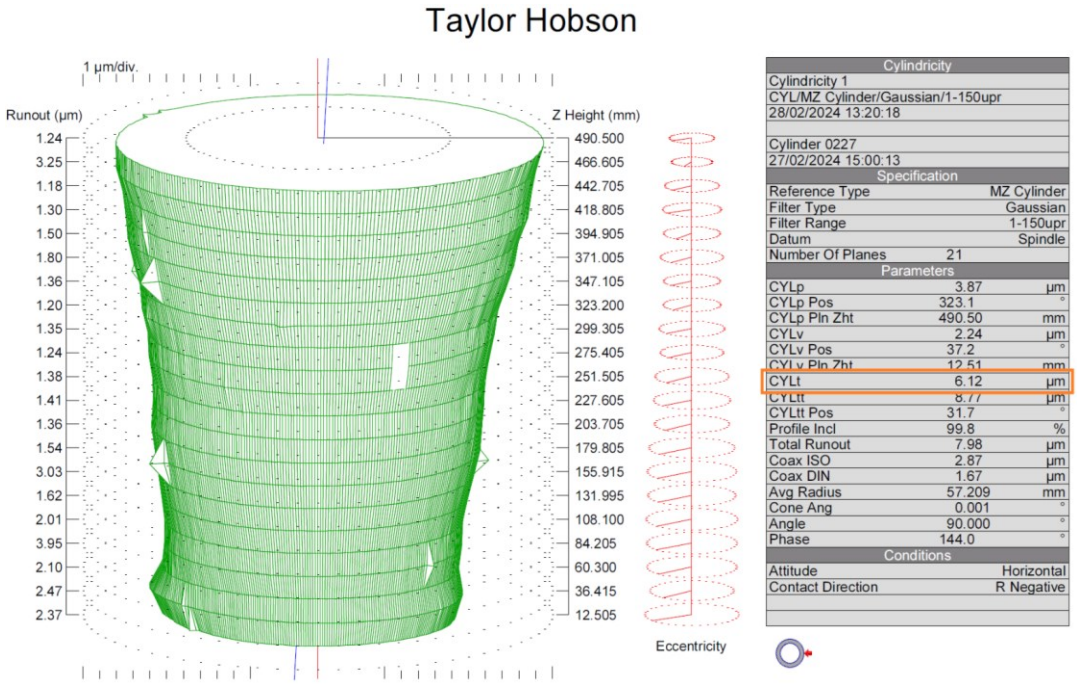

Figure 3.12: The cylindricity error, CYLt, in a typical measurement result of the cylinder standard, is 6.59 µm.

Therefore, the straight guide's inclination to the rotating spindle can be known by calculating the average cone angle. This can be done by first determining the cone angle for the upright cylinder standard and then for the upside-down cylinder. The average of these two cone angles represents the parallelism error between the spindle and the vertical straight guide. Figure 3.13 demonstrates the mathematical principle used to calculate the cone angle value. The half of the cone angle value can be obtained by:

$$\alpha = 90° - \beta \tag{3.1}$$

As we known, the slope (m) of the line AB is related to the angle (β) by the tangent function:

$$m = tan(\beta) \tag{3.2}$$

To find the angle β, the inverse tangent function can be used:

$$\beta = tan^{-1}(m) \tag{3.3}$$

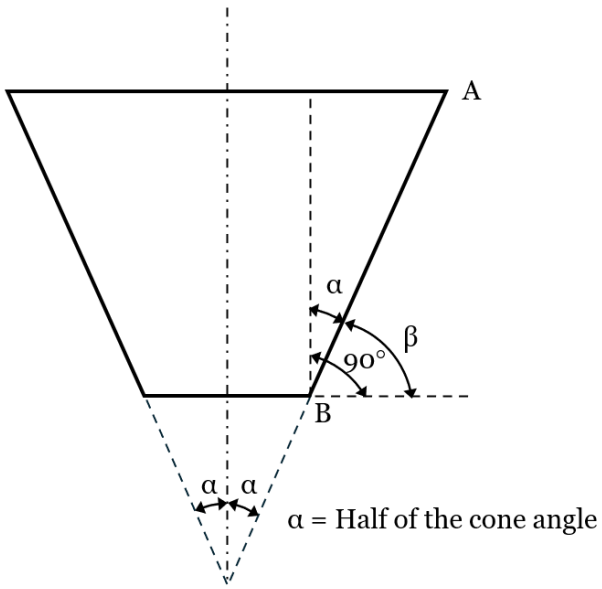

Figure 3.13: The mathematical principle used to calculate the cone angle value.

Considering that each of the 21 circular sections comprises 3,600 sampling points for a cylindricity measurement result, 3,600 vertical lines will be generated, each composed of points with the same point number across all 21 circular sections. For example, the first vertical line will consist of the first point from each of the 21 circular sections. Hence, a total of 3,600 cone angles will be analysed for both the upright cylinder standard and the upside-down cylinder, respectively.

Based on the analysis above, a MATLAB script (see Appendix C) was employed to calculate the average cone angle, which represents the parallelism error between the spindle and the vertical straight guide. Firstly, the measured roundness data at 21 circular sections, denoted as vectors *r1*, *r2*...r21 and *rud1*, *rud2*...rud21, were read. Then, two sets of 3,600 vertical lines were generated by using the MATLAB's `for` loop function for both the upright cylinder standard and the upside-down cylinder.

The least squares fitting was further applied to each set of vertical lines to achieve all corresponding slopes and offsets by using the MATLAB's `arrayfun` to call `polyfit` function for each vertical line. Subsequently, the average slope and offset for the upright cylinder standard were computed, resulting in vector '*slope_average'* and vector '*offset_average'*. As illustrated in Figure 3.14, all vertical lines for the upright cylinder were plotted in blue, along with their average fitting line depicted in red.

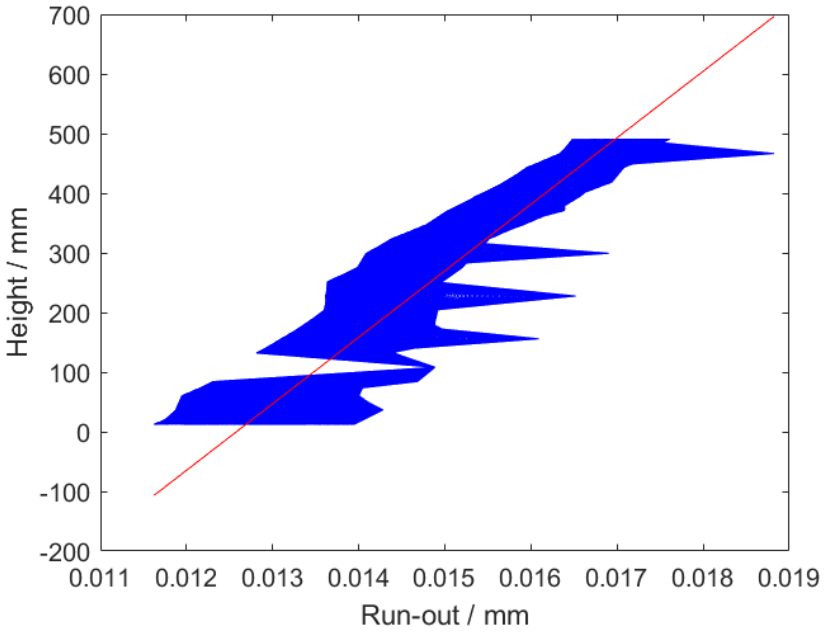

Figure 3.14: All vertical lines for the upright cylinder and their average fitting line.

Similarly, the average slope and offset for the upside-down cylinder were calculated, yielding vector *'slopeud_average'* and vector *'offsetud_average'*. Figure 3.15 shows all vertical lines for the upside-down cylinder in blue and their average fitting line in red.

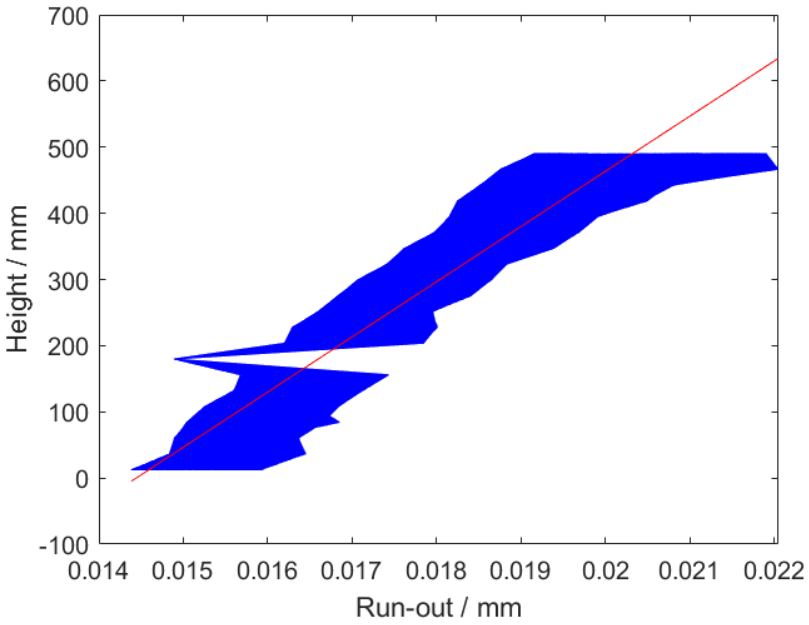

Figure 3.15: All vertical lines for the upside-down cylinder and their average fitting line.

Ultimately, the half of the cone angle value for the upright cylinder, denoted as vector *tilt_angle*, is only 0.00051°. Similarly, for the upside-down cylinder, the half-cone angle value, termed vector *tilt_angleud*, is a mere 0.00069°. Consequently, computing the average the half of cone angle, vector *tilt_anglefinal*, by averaging *tilt_angle* and *tilt_angleud*, yields a value of 0.00060°.

3.2.5 Evaluation of the column straightness error for Talyrond.

Straightness standards can be effectively employed to identify column straightness errors in cylindricity measuring machines. Any deviation from a perfectly straight line indicates errors in the column straightness, allowing for accurate assessment and potential correction of the straightness measurements.

Figure 3.16 demonstrates the measurement in which the probe is measuring the straightness of the straightness standard. During the experiment, the straightness standard was positioned along the axis of the rotary table firstly. Then, conducted the straightness measurement function of the Talyrond cylindricity measuring instrument five times and recorded the data. The measurements were taken at 1979 points from the height 18.5 mm to 503.11 mm.

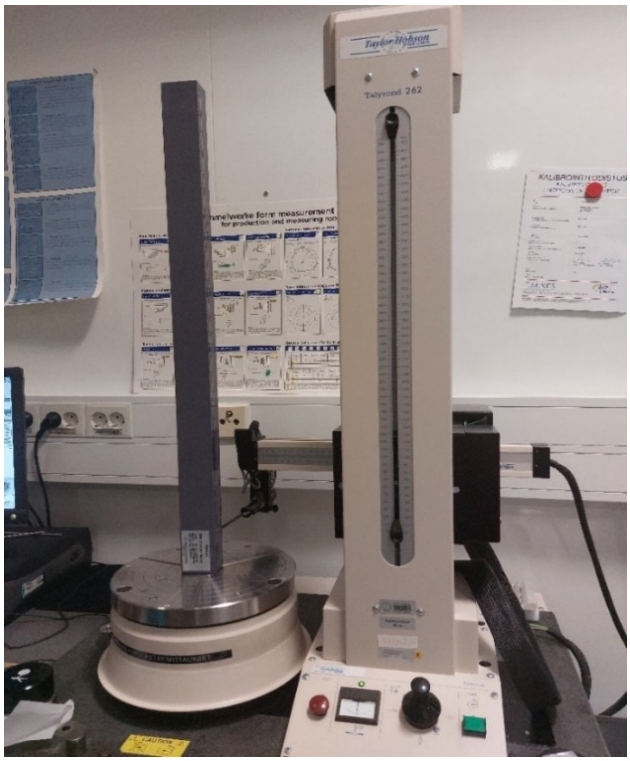

Figure 3.16: The probe is measuring the straightness of the straightness standard.

A typical measured straightness data of the straightness standard is illustrated in Figure 3.17. The error of the straightness obtained is 0.76 µm.

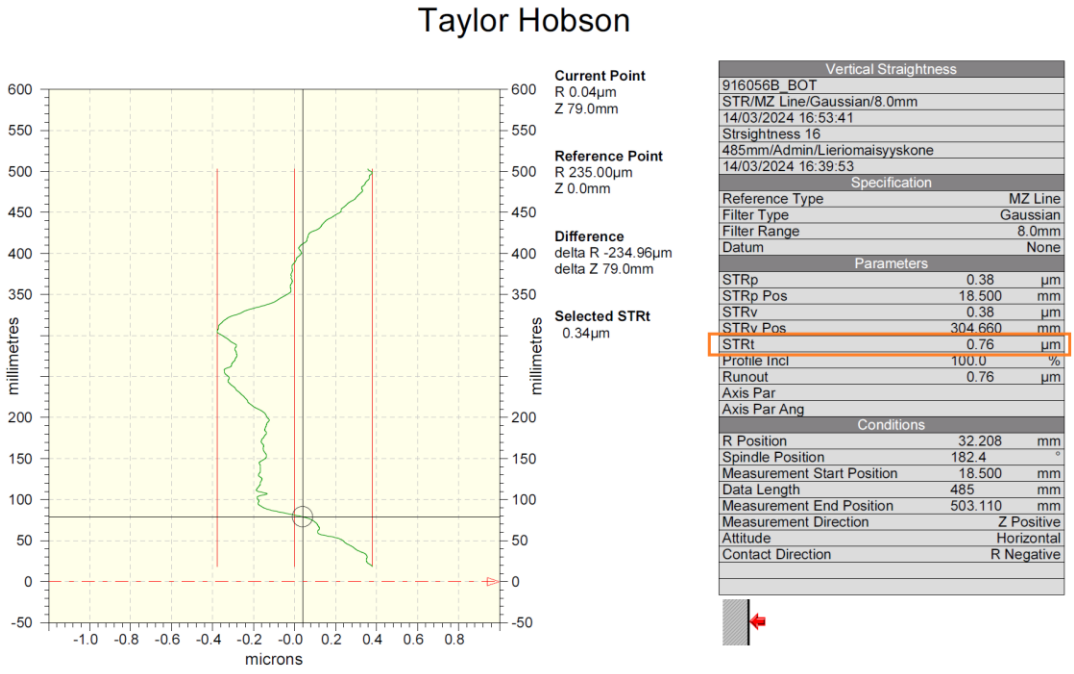

Figure 3.17: The measured straightness data of the straightness standard. The straightness error appears as the parameter STRt which is 0.76 µm, using a Gaussian filter with a range of 8 mm.

The measured straightness data was then analysed by using a MATLAB script. The detailed script is included in Appendix D. Initially, the measured straightness data, denoted as vectors *r1*, *r2*, *r3*, *r4*, and *r5*, were read. Subsequently, the average of the measured straightness data was calculated, denoted as vector *ravg*, and its least squares fitting line was computed using the MATLAB's `polyfit` function. The first and last 100 data points were excluded from analysis because of end effects in the gaussian filter and instability during acceleration at start and braking at the end.

In Figure 3.18, the average of the measured straightness data, *ravg*, is depicted in blue, while its corresponding least squares fitting line is obtained using MATLAB's `polyval` function, indicated in red colour. The straightness deviation can be calculated by subtracting the red line from the blue line.

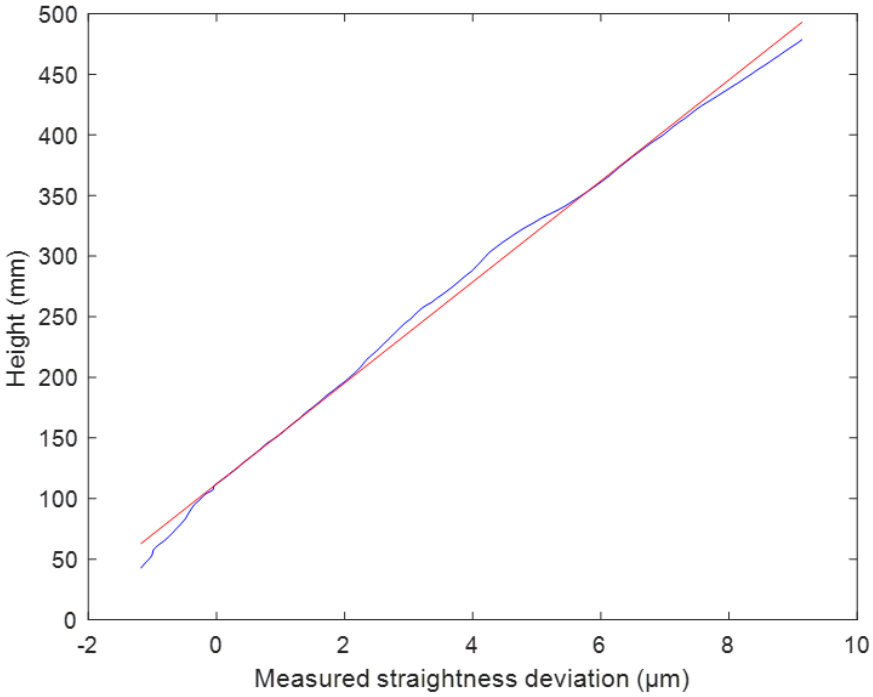

Figure 3.18: The measured straightness data from the point 101 to point 1879 (in the blue colour) and its least squares fitting line (in the red colour).

Finally, the straightness deviation of the column's vertical movement was calculated and subsequently plotted, as demonstrated in Figure 3.19.

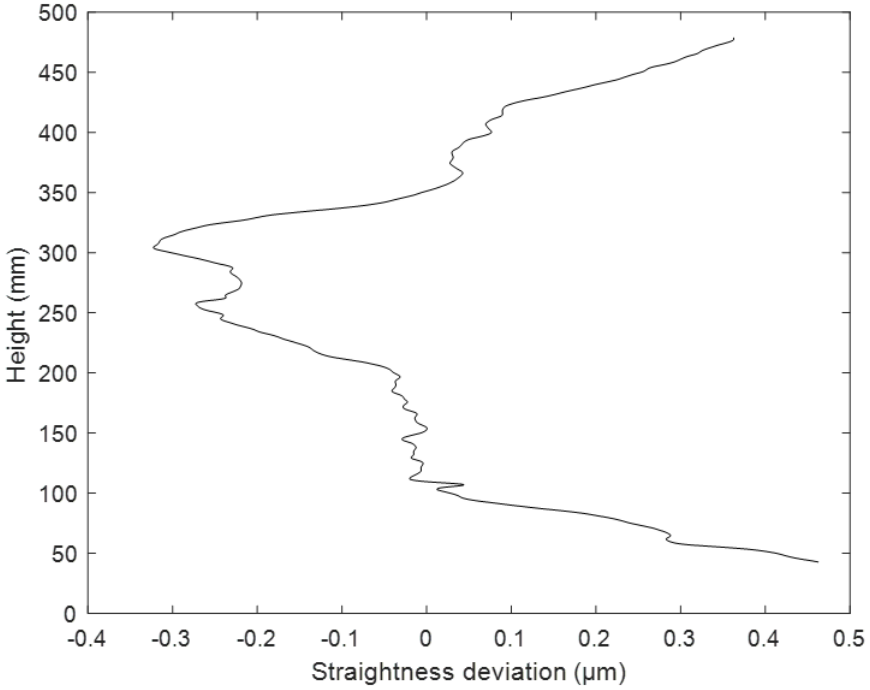

Figure 3.19: The straightness deviation of the column's vertical movement.

To determine the correction function for the straightness deviation of the vertical movement of column, Figure 3.19 underwent an adjustment in MATLAB by swapping the x-axis and y-axis. Y-axis represents the measure of straightness, while x-axis means the height. By using a MATLAB's 9th-degree polynomial function, a correction function for *y (straightness)* was generated:

$$y = -0.03788 * z^9 - 0.05796 * z^8 + 0.2922 * z^7 + 0.3836 * z^6 - 0.8089 * z^5 - 0.8126 * z^4 + 0.9132 * z^3 + 0.7696 * z^2 - 0.3169 * z - 0.2647 \quad (3.4)$$

Where z is:

$$z = \frac{(x - 260.7)}{125.9} \quad (3.5)$$

Based on the correction function defined above, a `straightness` function for the compensation of the straightness error was wrote, see Appendix D.

The correction function was then tested. In Figure 3.20, the plus sign ('+') means the correction values obtained by applying the correction function *y (straightness)* above. The differences between the deviation curve and the correction values are typically less than 0.06 μm, indicating the effectiveness of the correction function in illustrating the deviations.

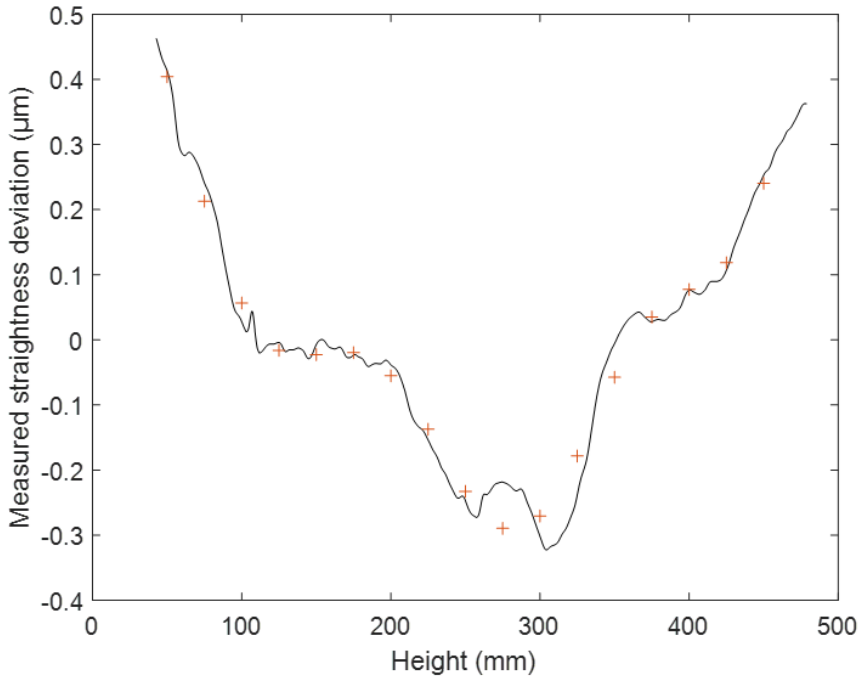

Figure 3.20: The measured straightness deviation and the correction values ('+') obtained by applying the correction function *y* for 17 heights.

4 Results

4.1 Comparison between measured results and specification from manufacturer

4.1.1 Error of rotary table

The error specification for the radial error of the rotary table is defined as within 0.04 μm + 0.0003 μm/mm height above the worktable. Since the roundness of glass hemisphere was measured at the height of 75 mm, the corresponding radial error of the rotary table should be within 0.0625 μm. In the conducted measurements, the recorded result is 0.048 μm (refer to Figure 3.5).

Meanwhile, the maximum axial movement of worktable during one resolution is 0.06μm according to manufacturer. In the performed measurements the result, FLTt, is 0.03 μm, as shown in Figure 3.8.

4.1.2 Probe

According to manufacturer's specifications, the linearity of the probe is ±0.1% over ±0.2 mm. However, the measured deviation of the probe in Table 5 was found to be between ±2%and ±3%, significantly exceeding the specified linearity of the probe.

4.1.3 Parallelism

According to the manufacturer's specifications, the parallelism to spindle axis for the column with a length of 500 mm in the measuring plane is 5 μm over 500 mm. Based on Figure 3.14 and Figure 3.15, the recorded result slightly exceeded 5 μm, reaching approximately 7 μm.

4.1.4 Straightness

According to Table 2, the Straightness Limit of Error is 1.5 μm over 500 mm and 0.25 μm over any 100 mm length. In the performed measurements the result of Figure 3.17, the straightness error, STRt, is 0.76 μm over the length of 466.5 mm. It complies satisfactorily with the specification for 500 mm. Furthermore, by analysing data from the Figure 3.19, it seems that the requirement of 0.25 μm over any 100 mm length is exceeded both at the lower and upper parts of the column.

Table 6 demonstrates the detailed specifications from the manufacturer, the measured results, and the comparison between them in terms of the rotary table, probe, parallelism to spindle axis, and straightness.

Table 6: Comparison between measured results and specification from manufacturer.

Error Source	Specification	Measured result	Comparison
Radial error of the table	within 0.0625 μm	0.048 μm	Comply with the specification.
Axial movement of worktable	0.06 μm maximum axial movement of worktable during one resolution	FLTt, 0.03 μm	Comply with the specification.
Linearity of the probe	±0.1% over ±0.2 mm	between ±2%and ±3%	Significantly exceeding the specified linearity of the probe.
Parallelism to spindle axis	5 μm over 500 mm	7 μm	slightly exceeded 5 μm.
Straightness Error	1.5 μm over 500 mm and 0.25 μm over any 100 mm length	STRt is 0.76 μm over 466.5 mm	Comply with the requirement of 1.5 μm over 500 mm. But the requirement of '0.25 μm over any 100 mm length' is exceeded both at the lower and upper parts of the column.

4.2 Compensation of angle and straightness errors

Using the known errors of the instrument, the following describes how these can be compensated for angle and straightness errors. It should be noted that in the normal use of the instruments its software does both filtering and cylindrical fitting. As the compensation is done in MATLAB both filtering and cylindrical fitting must be implemented in MATLAB.

Firstly, the measured roundness data (*r1*, *r2*...*r21*) were read and the measured cylinder was plotted by calling the MATLAB's `pol2cart` function.

Then, the `straightness` function above was used to obtain the compensated roundness data. Similarly, an `angle` function for the compensation of the angle error was created, as shown in Appendix E.

Next, the compensated roundness at the *z* height can be achieved by:

$$r\_comp(z) = r + angle(height(z)) + straightness(height(z)) \qquad (4.1)$$

Following that, a mathematical representation of cylindrical form can be used to identify the best-fit cylindrical shape. Muralikrishnan and Raja (2009, p.148) described that "Let z be the height, and e and f be the tilt parameters of the axis, and the limaçoid cylinder can then be represented by:

$$R(\theta, z) = r + (a + ze)cos\theta + (b + zf)sin\theta \qquad (4.2)$$

where functional relationship of R to θ and z is expressed as $R(\theta\ ,\ z)$. "

The parameters of the limaçoid cylinder in Eq. (4.2) will be assessed by employing the MATLAB's `limacoid` function, as shown in the MATLAB script in Appendix E. Ultimately, the compensated cylinder, centring by using eccentricity values, was generated.

Figure 4.1 shows the measured cylinder by the uncorrected data from the cylindricity measuring machine.

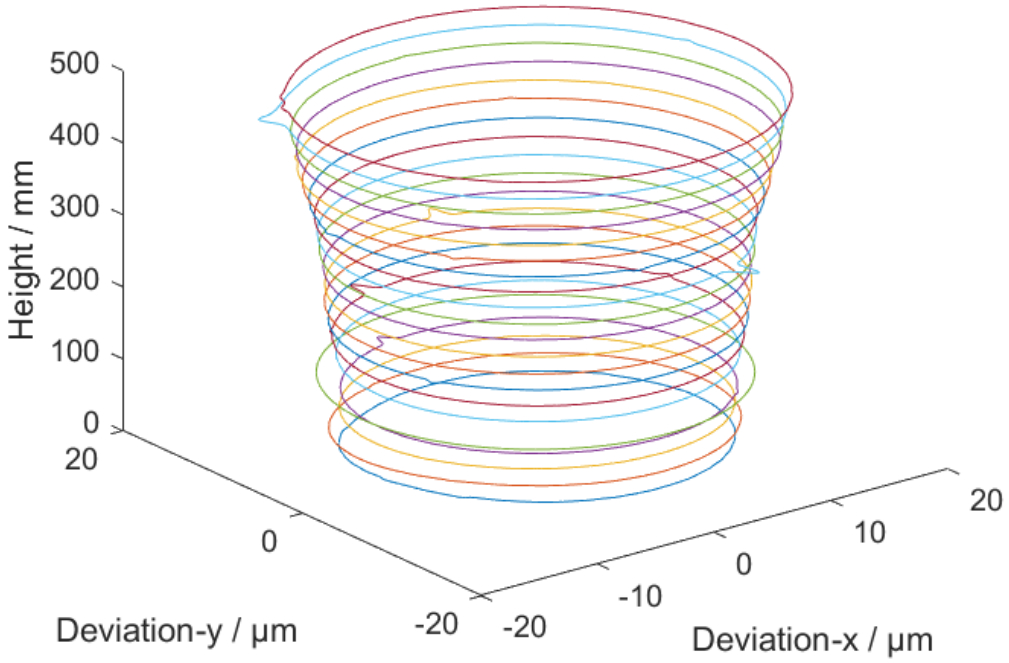

Figure 4.1: The measured cylinder.

Figure 4.2 illustrates the compensated cylinder achieved through the correction of both angle and straightness errors.

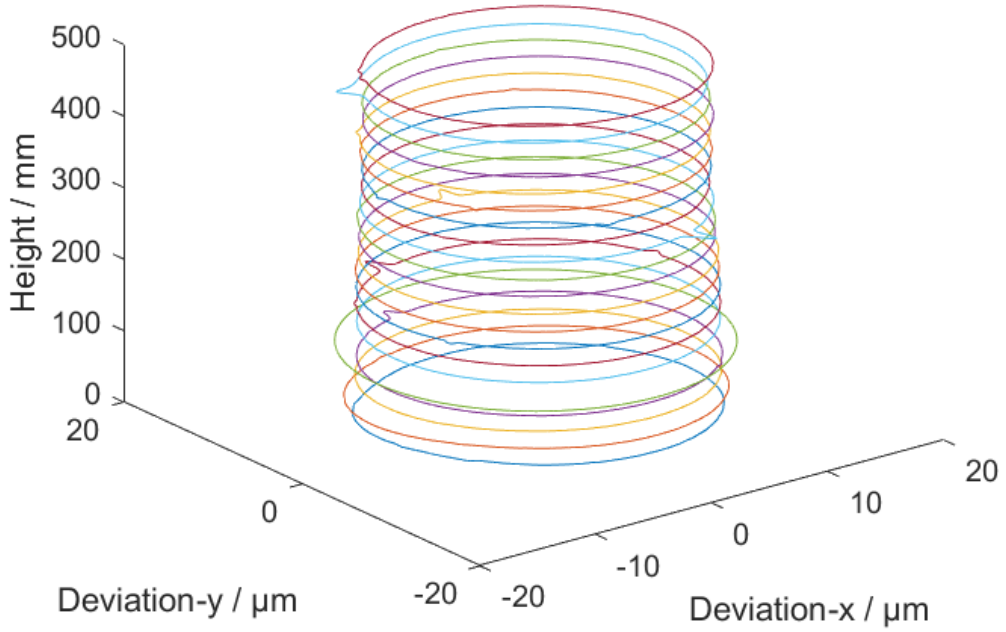

Figure 4.2: The compensated cylinder.

Noticeably, the cylindrical error for the compensated cylinder, *CYLt*, is reduced from 6.59 µm to 4.73 µm, which is an improvement for the cylindricity measurement.

4.3 Evaluation of measurement uncertainty for cylindricity

In this part, the principle described in section 2.1.1 is followed for the evaluation of the measurement uncertainty.

4.3.1 Measurement model

Measured point at radius R at angle θ and height z is a function of several input quantities. By applying notation from Haitjema (2001), the measurement model can be written as:

$$R(\theta, z) = f(m_1, m_2, \dots m_n) \tag{4.3}$$

The input quantities $m_1 \ldots m_n$ represent the dimensions and form of the cylinder together with error sources and uncertainties. This measurement model gives the measured point cloud consisting of thousands of points. For simplicity effects of filtering and best fit are not considered in this uncertainty analysis.

Neugebauer (2001) provided a method for calculating the uncertainty for roundness parameter RONt, which can now be adapted for determining the cylindricity parameter deviation CYLt. The CYLt can be obtained by considering the maximum and minimum profile points, denoted as *Pmax* and *Pmin* respectively:

$$P = R(\theta, z) \tag{4.4}$$

$$Pmax = max(R(\theta, z) \tag{4.5}$$

$$Pmin = min(R(\theta, z) \tag{4.6}$$

Thus, CYLt is determined as the difference between *Pmax* and *Pmin*:

$$CYLt = Pmax - Pmin \tag{4.7}$$

To achieve this, the correlation between these two points needs to be determined. For simplification, complete correlation between the maximum and minimum profile points will be assumed (Neugebauer, 2001). The uncertainty of the cylindricity deviation parameter *u(CYLt)* is the combined uncertainties of both the maximum and minimum profile points:

$$u(CYLt) = u(Pmax) + u(Pmin) \tag{4.8}$$

Assuming that the profile points' uncertainties are uniform across the circumference, we get:

$$u(CYLt) = 2\,u(R(\theta, z) \tag{4.9}$$

4.3.2 Error of rotary table

The radial error of the rotary table is 48 nm according to the Figure 3.5. It is assumed that it has a rectangular distribution, the corresponding half-width is 24 nm. Therefore, the standard uncertainty of the rotary table is:

$$\frac{24\ \text{nm}}{\sqrt{3}} = 0.014\ \mu\text{m}$$

4.3.3 Probe

The deviation of the probe is identified pessimistically within 2.86% (see Table 5). It is assumed to conform to a rectangular distribution. The roundness deviation of the cylinder standard is assumed to be less than 5 µm. According to the Eq. (2.2), the standard uncertainty for the probe is:

$$\frac{2.86\%}{\sqrt{3}}(5\ \mu\text{m}) = 1.6512\%(5\ \mu\text{m}) = 0.083\ \mu\text{m}$$

4.3.4 Parallelism deviation

The parallelism deviation is identified from measurements of the cylinder standard. From the results of the section 3.2.4 the evaluated half of the cone angle is 0.00060°. For the uncompensated case, the half of the cone angle is assumed to be within ±0.00060°. The standard uncertainty for the parallelism deviation is approximated to be 0.00001 rad, assuming no statistical distribution.

4.3.5 Straightness deviation

The straightness deviation is determined from measurements of the straightness standard. From the results in Figure 3.17, the straightness deviation is 0.76 µm. Assuming it follows a rectangular distribution, and its corresponding half-width for the straightness deviation is 0.38 µm. Therefore, the standard uncertainty of the straightness deviation is estimated to be:

$$\frac{0.38\ \mu\text{m}}{\sqrt{3}} = 0.219\ \mu\text{m}$$

4.4 Measurement uncertainty without error compensation

For purpose of comparison measurement, uncertainty for cylindricity without error compensation is presented in Table 7. It represents the case where the corrections presented in section 3.2 are not applied. The found parallelism deviation is used as the standard uncertainty. While this is not entirely accurate, it provides a useful approximation of the uncertainty magnitude without error compensation.

Table 7: The evaluation of measurement uncertainty for cylindricity without error compensation. L is the height of the cylinder.

Parameter	Distribution	Standard Uncertainty	Sens. Coefi.	Uncertainty contribution
Radial error of table	rectangular	0.014 μm	1.0	0.014 μm
Probe	rectangular	0.083 μm	1.0	0.083 μm
Parallelism deviation	non statistical	0.00001 rad	L	0.00001 L
Straightness deviation	rectangular	0.219 μm	1.0	0.219 μm
	Independent of length			0.235 μm
	Length dependent			0.00001 L
	Expanded uncertainty (k=2)			Q [0.47; 0.000021L] μm, L in μm
	Expanded uncertainty (k=2)			Q [0.47; 0.021L] μm, L in mm

4.5 Measurement uncertainty with error compensation

Based on the compensation for the identified straightness deviation and parallelism deviation by using MATLAB script, the evaluation of measurement uncertainty for cylindricity with error compensation can be obtained, summarised in Table 8.

Since error compensation is not applied to the probe and the error of the rotary table, the uncertainties of them remain unchanged.

From the Figure 3.14 and Figure 3.15, the half of the cone angle is approximated to 0.00060°± 0.000035°, assuming a rectangular distribution. The standard uncertainty for the parallelism deviation is calculated by dividing 0.000035° by the square root of 3, yielding 0.000020°. Finally, the standard uncertainty of the mean in degrees is obtained by dividing 0.000020° by 7200 (the total number of half cone angles), which approximates to 4.2×10^{-9} rad, as derived using Eq. (2.1).

Considering the compensation for the straightness deviation, the uncompensated straightness deviation is less than 0.06 μm, as shown in Figure 3.20. By assuming a rectangular distribution, the associated standard uncertainty is 0.035 μm which is obtained by dividing 0.06 μm by square root 3. The error of straightness according to the certificate is 0.13 μm.

Table 8: The evaluation of measurement uncertainty for cylindricity with error compensation. L is the height of the cylinder.

Parameter	**Distribution**	**Standard Uncertainty**	**Sens. Coefi.**	**Uncertainty contribution**
Radial error of table	rectangular	0.014 μm	1.0	0.014 μm
Probe	rectangular	0.083 μm	1.0	0.083 μm
Uncompensated Paral-lelism deviation	rectangular	$4.2x10^{-9}$ rad	L	$4.2x10^{-9}$ L
Uncompensated Straightness deviation	rectangular	0.035 μm	1.0	0.035 μm
	Independent of length			0.091 μm
	Length dependent			$4.2x10^{-9}$ L
	Expanded uncertainty (k=2)			Q [0.18; 0.0000000083L] μm, L in μm
	Expanded uncertainty (k=2)			Q [0.18; 0.0000083L] μm, L in mm

5 Conclusions

This thesis is dedicated to answer the two research questions. Firstly, it aims to identify the sources of error in cylindricity measurement within calibration laboratory settings and subsequently quantify these error sources. Additionally, Furthermore, it seeks to investigate error compensation methods for minimizing the influence of these errors through the implementation of error separation techniques.

Through meticulous investigation, this thesis has identified four key sources of error in cylindricity measurement within a calibration laboratory: the error of the rotary table, precision of the probe, parallelism error to the spindle axis, and column straightness error. Employing an error separation method alongside MATLAB script, these error sources have been quantified and minimized.

For instance, to assess the rotary table, a multi-step four-position error separation method was employed to identify radial error, while axial error was determined by measuring the flatness of a glass hemisphere. The results revealed that the measured errors of the rotary table are small, the measured radial error of 0.048 μm that falls within acceptable limits, the specified limit of 0.0625 μm by manufacturer.

The precision of the probe was scrutinized. It involved determining an optimal probe angle of 5° and identifying a correction factor through multiple rounds of measurements on flick standards with nominal depths of 2.55 μm, 12.20 μm, and 23.10 μm. Although the achieved probe error of between ±2% and ±3% is larger than the specified linearity limit of ±0.1% over ±0.2 mm in manufacturer specification, it has been known earlier and can be acceptable. This is because in most measurement tasks the parts to be measured typically have roundness errors below 5 μm making this relatively large error to be small in practice.

Additionally, the significant parallelism deviation and straightness error were carefully evaluated. The parallelism to spindle axis was found to be considerable. In this work, upside-down error separation was done, and the result is that the measured parallelism of 7 μm slightly exceeds the specified limit of 5 μm over 500 mm.

On the other hand, the straightness error evaluation reveals that the overall straightness error (STRt) of 0.76 μm over 466.5 mm complies with the specified limit of 1.5 μm over 500 mm, but the requirement of 0.25 μm over any 100 mm length is exceeded at both the lower and upper parts of the column.

Despite the identified errors, this thesis offers practical solutions for minimizing their influence on cylindricity measurements. The error of the parallelism to spindle axis can be compensated by applying a MATLAB's `angle` function to the found angle error. Meanwhile, the straightness error can be compensated by using the correction function Eq. (3.4) and Eq. (3.5). These compensation methods effectively mitigate the impact of error sources, enhancing overall measurement accuracy in calibration laboratory settings.

In conclusion, the discovery in this thesis not only builds upon existing knowledge but also offers practical solutions to enhance the accuracy and reliability of cylindricity measurements in calibration laboratories. The findings will be utilized for cylindricity measurements at VTT MIKES in the future, and corresponding instructions have been documented as part of the instruction collections at VTT MIKES. The methods and MATLAB script developed in this thesis can be also used by other users or industries. It contributes to the continuous improvements and refinement of measurement techniques, providing insights for future research and applications in industries.

References

Aamir, M. (2021) *Simultaneous machining of aerospace structural materials using poly-drills*. PhD thesis. Edith Cowan University.

Bell, S. (2001) '*A Beginner's Guide to Uncertainty of Measurement Measurement Good Practice Guide*'.

Cao, L.X. *et al.* (1992) 'Full-harmonic error separation technique', *Measurement Science and Technology*, *3*(12), p.1129.

EMI Gage (no date) *Data_Sheet_Talyrond262*. Available at: https://www.emigage.com/PDF%20Files/Data_Sheet_Talyrond262.pdf (Accessed 3 May 2024).

Finnish Standards Association (2006) *SFS-EN ISO 1101 – Geometrical Product Specifications (GPS). Geometrical tolerancing. Tolerances of form, orientation, location and run-out*, SFS.

Grejda, R., Marsh, E. and Vallance, R. (2005) 'Techniques for calibrating spindles with nanometer error motion', *Precision Engineering*, 29(1), pp. 113–123.

Haitjema, H. *et al.* (2001) 'Virtual CMM using Monte Carlo methods based on frequency content of the error signal', SPIE Proceedings, 4401, pp. 158-167.

Howarth, P. *et al* (2008) "metrology–in short" 3rd edition. *EURAMET project*, *1011*.

International Organization for Standardization (2011) *ISO 12180-1:2011 geometrical product specifications (gps). cylindricity. part 1: vocabulary and parameters of cylindrical form,* ISO.

Kumar, S. *et al.* (2022) 'Roundness of a Flick Standard and Analyzing Effects of Different Filters While Using Least Squares Reference Circle Method of Roundness Measurement', *Advances In Metrology,* pp. 159-167.

Lao, Y.Z. *et al.* (2003) 'Accurate cylindricity evaluation with axis-estimation preprocessing', *Precision Engineering*, 27(4), pp. 429–437.

Marsh, E.R., Arneson, D.A. and Martin, D.L. (2010) 'A comparison of reversal and multiprobe error separation', *Precision Engineering*, 34(1), pp. 85–91.

Muralikrishnan, B. and Raja, J. (2009) *Computational surface and roundness metrology*. London: Springer.

Mitutoyo Europe (no date) *Roundtest RA-2200AH*. Available at: https://shop.mitutoyo.eu/web/mitutoyo/en/mitutoyo/04.03.01.05/R

oundtest%20RA-2200AH/$catalogue/mitutoyoData/PR/211-512-11/index.xhtml;jsessionid=F0347870CD66A5BEE1C9607185E0A436/ (Accessed 3 May 2024).

Neugebauer, M. (2001) 'Uncertainty analysis for roundness measurements by the example of measurements on a glass hemisphere', *Measurement Science and Technology*, *12*(1), pp.68.

Schmitt, R.H. *et al.* (2016) 'Advances in Large-Scale Metrology – Review and future trends', *CIRP Annals - Manufacturing Technology*, 65(2), pp. 643–665.

Sun, T. (1996) 'Two-step method without harmonics suppression in error separation', *Measurement Science and Technology*, *7*(11), pp.1563.

Taylor Hobson (no date) *Exploring Roundness A fundamental guide to the measurement of cylindrical form*. Available at: https://www.taylor-hobson.com.cn/-/media/ametektaylorhobson/files/learning-zone/chinese/books/exploring-roundness.pdf?revision=34b3ea99-3db6-4042-9bd2-7041ae234ee6 (Accessed 20 May 2024).

Vissiere, A. *et al.* (2013) *Mesure de cylindricité de très haute exactitude. Développement d'une nouvelle machine de référence*. Doctoral dissertation. École doctorale Sciences des métiers de l'ingénieur (Paris).

Xue, Z. and Ye, X. (2006) 'Cylindricity compound errors reversal separation method', *SPIE Proceedings*, 6357, pp. 446-452.

Yang, R. *et al.* (2023) 'A Novel Cylindricity Measurement Method for Large Workpiece Based on Improved Model and Algorithm', *IEEE Transactions on Instrumentation and Measurement*.

Zhao, F., Zhang, L. and Zheng, P. (2010) 'Estimation of the uncertainty propagation in verification operator of cylindricity errors', *SPIE Proceedings*, 7544, pp. 64-71.

Appendix

Appendix A: The centering of the cylindricity measuring machine

A 110 G7 plug gauge was measured by using Taylor Hobson cylindricity measuring machine in the laboratory 010Pit of VTT MIKES. The axis of the plug gauge was firstly aligned with the axis of the rotary worktable by means of a centring and levelling table, as shown in Figure A.1. It involved that the plug gauge is placed at the centre of the rotary worktable, ensuring close proximity of the stylus to the surface earmarked for measurement. Observations were made on the variations in distance between the stylus and the plug gauge while manually turning the worktable. The alignment adjustment of the plug gauge was accomplished by tapping on the surface with the handle of a screwdriver. Following this, the precise centring of the plug gauge was automated through the software by selecting the sequence "adjusted->home->all."

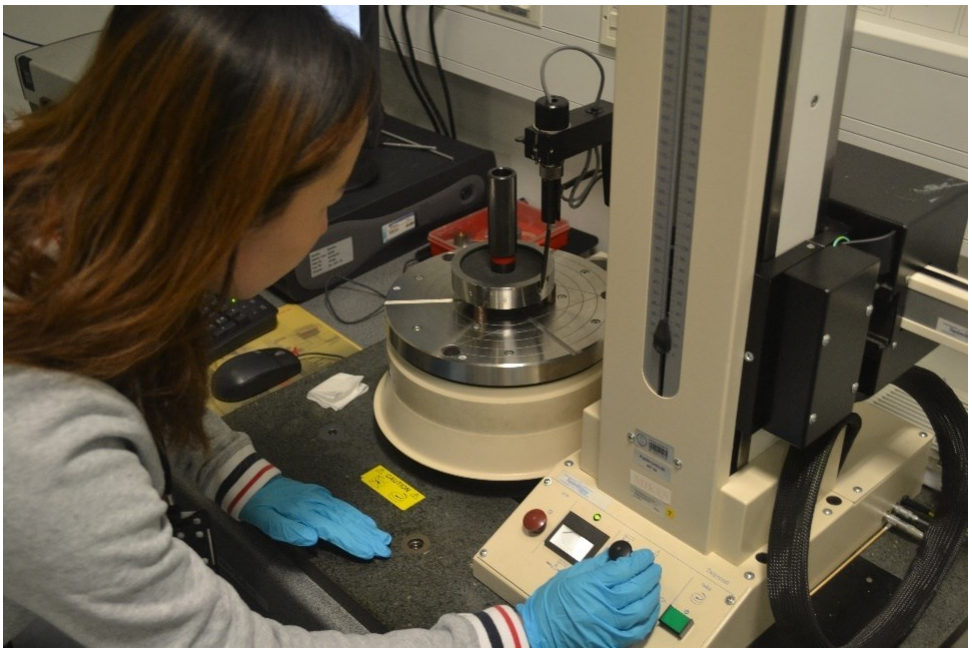

Figure A.1: Adjusting the plug gauge to be coaxial with the rotary worktable.

The centring procedure for the plug gauge required execution at two distinct plane levels. Firstly, the stylus was moved from the bottom edge to the top edge of the surface to obtain the total height of the measured component, covering a distance of 24 mm. Next, by selecting the “Talyrond->reset”, the middle line of the surface was established as the 0 mm reference point when the stylus was positioned on the centre line of the surface. Then, the stylus was moved to a height of 4 mm. Finally, utilizing the software commands

"Adjusted->Auto centre and level->Level separation: 16 mm," the cylinder to be measured was effectively centred on the rotary worktable.

After the centring process, the extra measurement was performed by selecting three planes spaced at 8 mm intervals, as illustrated in Figure A.2. The measurement result is described in Figure A.3.

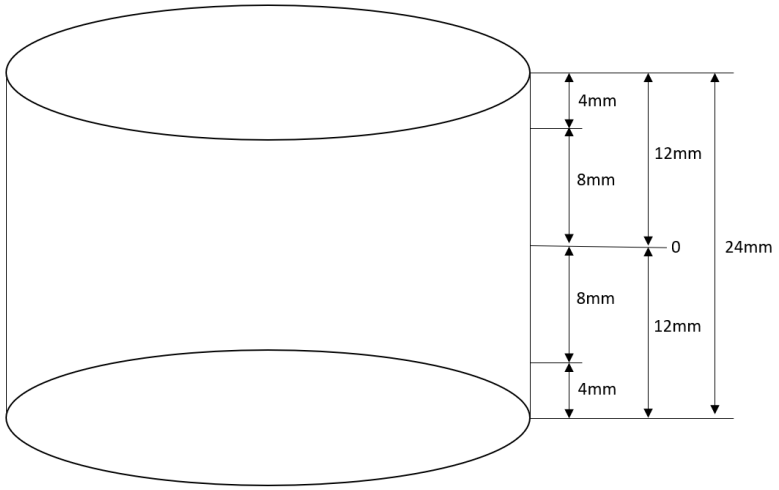

Figure A.2: The three planes selected for auto centre and level.

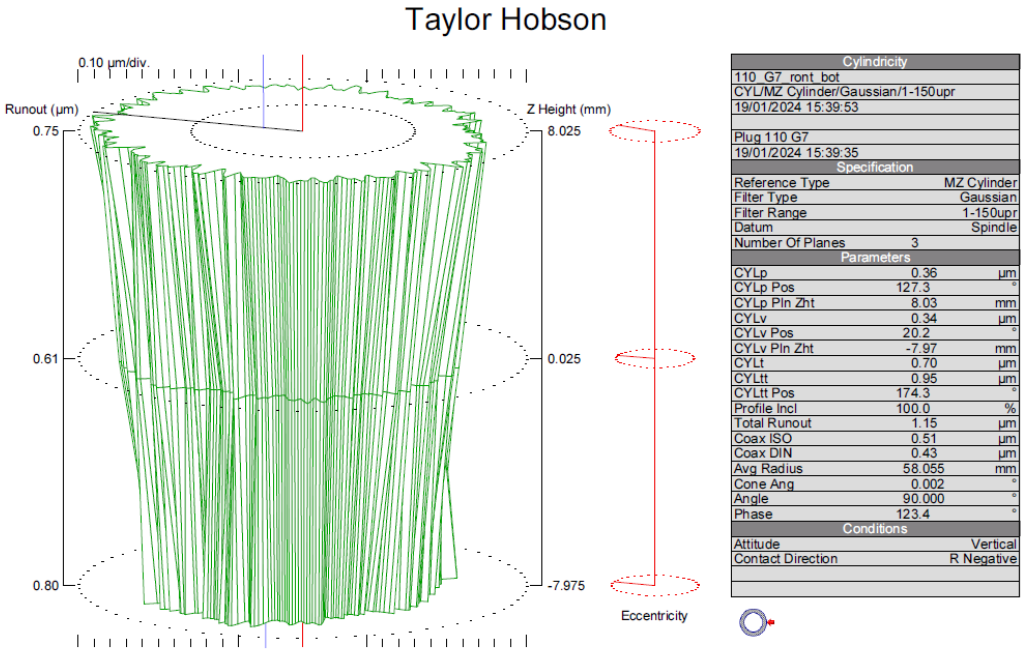

Figure A.3: The measurement result of the plug gauge cylinder.

Three cylindrical planes are depicted in the Figure A.4, Figure A.5 and Figure A.6 respectively.

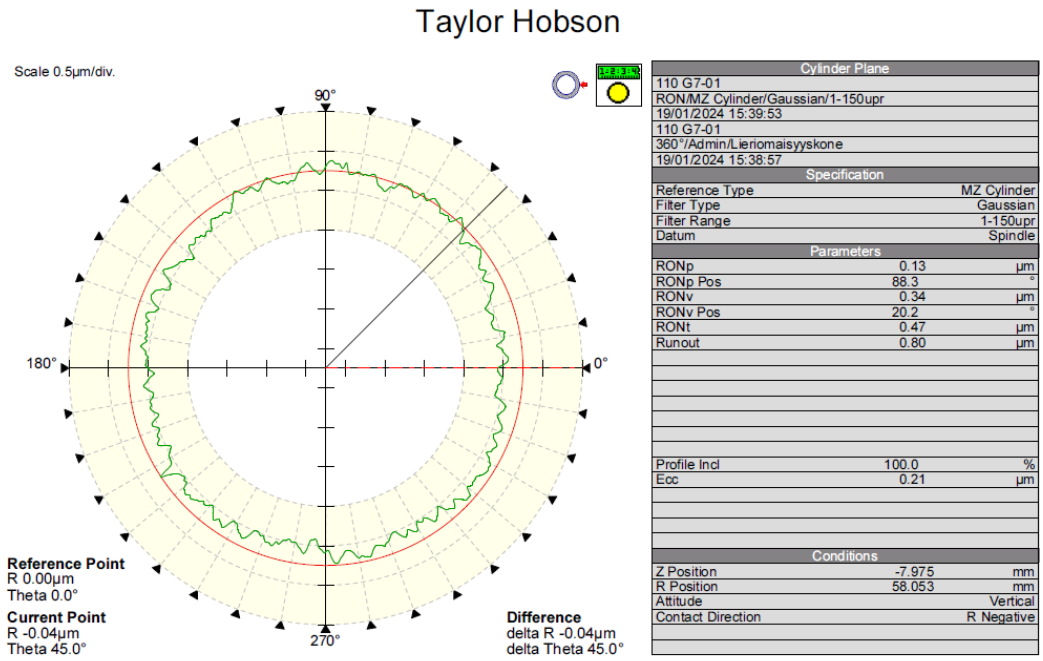

Cylinder Plane		
110 G7-01		
RON/MZ Cylinder/Gaussian/1-150upr		
19/01/2024 15:39:53		
110 G7-01		
360°/Admin/Lieriomaisyyskone		
19/01/2024 15:38:57		
Specification		
Reference Type		MZ Cylinder
Filter Type		Gaussian
Filter Range		1-150upr
Datum		Spindle
Parameters		
RONp	0.13	µm
RONp Pos	88.3	°
RONv	0.34	µm
RONv Pos	20.2	°
RONt	0.47	µm
Runout	0.80	µm
Profile Incl	100.0	%
Ecc	0.21	µm
Conditions		
Z Position	-7.975	mm
R Position	58.053	mm
Attitude		Vertical
Contact Direction		R Negative

Figure A.4: The cylinder planes at the height of 4 mm.

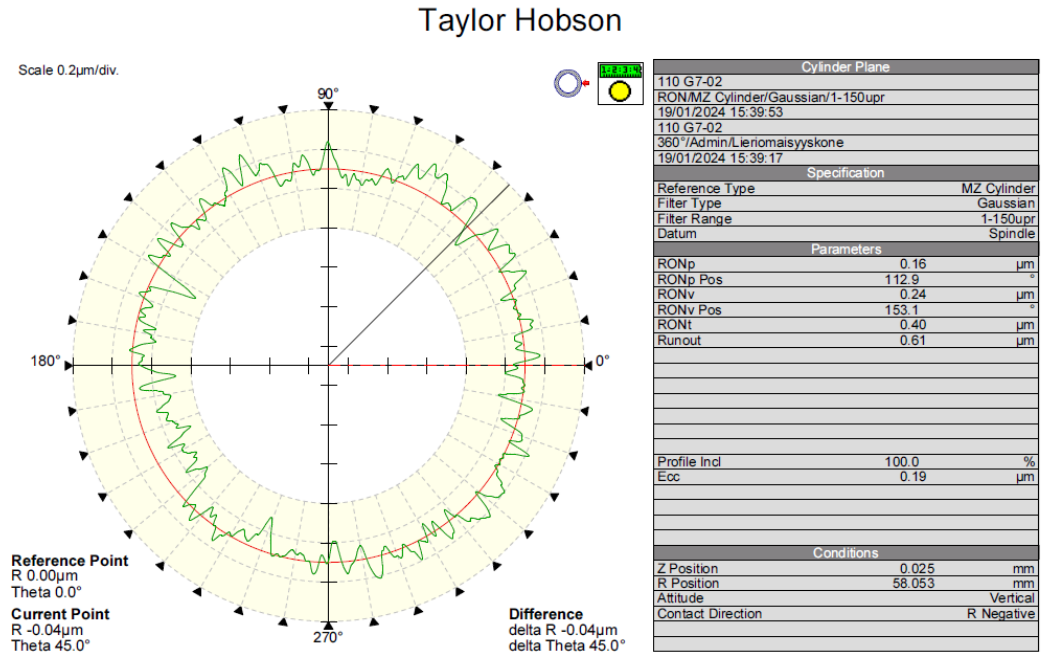

Cylinder Plane		
110 G7-02		
RON/MZ Cylinder/Gaussian/1-150upr		
19/01/2024 15:39:53		
110 G7-02		
360°/Admin/Lieriomaisyyskone		
19/01/2024 15:39:17		
Specification		
Reference Type		MZ Cylinder
Filter Type		Gaussian
Filter Range		1-150upr
Datum		Spindle
Parameters		
RONp	0.16	µm
RONp Pos	112.9	°
RONv	0.24	µm
RONv Pos	153.1	°
RONt	0.40	µm
Runout	0.61	µm
Profile Incl	100.0	%
Ecc	0.19	µm
Conditions		
Z Position	0.025	mm
R Position	58.053	mm
Attitude		Vertical
Contact Direction		R Negative

Figure A.5: The cylinder planes at the height of 12 mm.

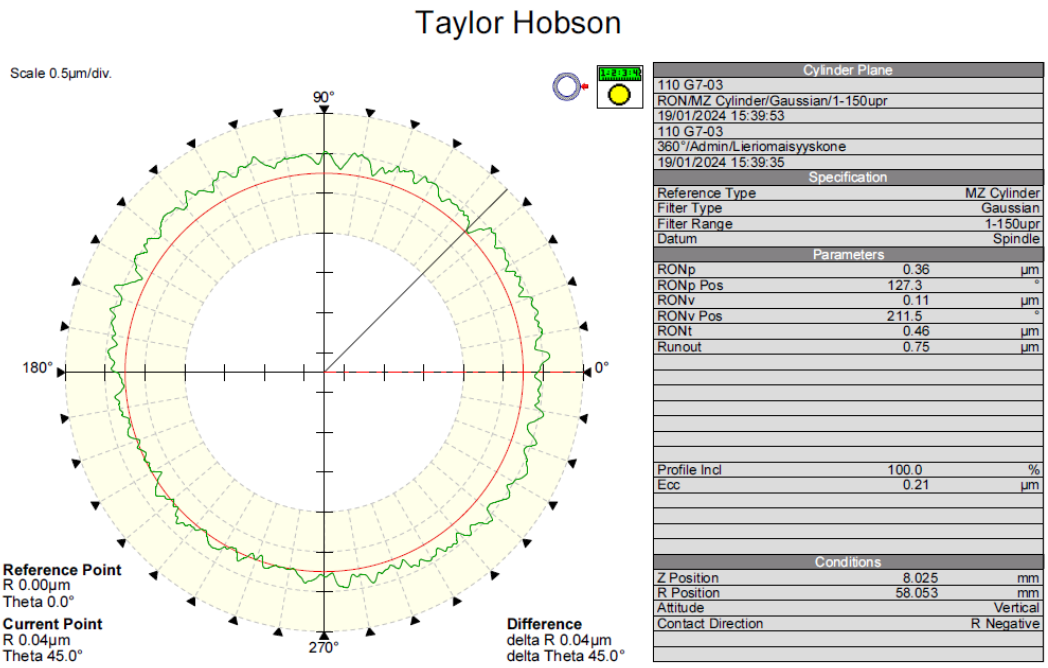

Figure A.6: The cylinder planes at the height of 20 mm.

Appendix B: The MATLAB script of the four-position method

```
close all
clear all
ra1=Read_PLN('Glass 786 a 1.PLN');
ra2=Read_PLN('Glass 786 a 2.PLN');
ra3=Read_PLN('Glass 786 a 3.PLN');
ra4=Read_PLN('Glass 786 a 4.PLN');
ra5=Read_PLN('Glass 786 a 5.PLN');
avga=(ra1+ra2+ra3+ra4+ra5)/5;
%ra6=Read_PLN('Glass 786 a 6.PLN');
%ra7=Read_PLN('Glass 786 a 7.PLN');
rb1=Read_PLN('Glass 786 b 1.PLN');
rb2=Read_PLN('Glass 786 b 2.PLN');
rb3=Read_PLN('Glass 786 b 3.PLN');
rb4=Read_PLN('Glass 786 b 4.PLN');
rb5=Read_PLN('Glass 786 b 5.PLN');
avgb=(rb1+rb2+rb3+rb4+rb5)/5;
avgb_con=[avgb;avgb];
start_point = 901;
end_point = 4500;
shiftedavgb = avgb_con(start_point:end_point);

rc1=Read_PLN('Glass 786 c 1.PLN');
rc2=Read_PLN('Glass 786 c 2.PLN');
rc3=Read_PLN('Glass 786 c 3.PLN');
rc4=Read_PLN('Glass 786 c 4.PLN');
rc5=Read_PLN('Glass 786 c 5.PLN');
avgc=(rc1+rc2+rc3+rc4+rc5)/5;
avgc_con=[avgc;avgc];
start_point = 1801;
end_point = 5400;
shiftedavgc = avgc_con(start_point:end_point);

rd1=Read_PLN('Glass 786 d 1.PLN');
rd2=Read_PLN('Glass 786 d 2.PLN');
rd3=Read_PLN('Glass 786 d 3.PLN');
rd4=Read_PLN('Glass 786 d 4.PLN');
rd5=Read_PLN('Glass 786 d 5.PLN');
avgd=(rd1+rd2+rd3+rd4+rd5)/5;
avgd_con=[avgd;avgd];
start_point = 2701;
end_point = 6300;
shiftedavgd = avgd_con(start_point:end_point);

offset=0.4;
n=3600;
i=1:n;
fi=(i/n*2*pi)';
polar(fi,avga-offset,'r');
hold on
polar(fi,avgb-offset,'b');
polar(fi,avgc-offset,'g');
```

```
polar(fi,avgd-offset,'y');
RTe=(avga+avgb+avgc+avgd)/4;
RTee=max(RTe)-min(RTe);
polar(fi,RTe-offset,'k');
title(RTee);
legend('avga','avgb', 'avgc','avgd','RTe')
figure
polar(fi,avga-offset,'r');
hold on
polar(fi,shiftedavgb-offset,'b');
polar(fi,shiftedavgc-offset,'g');
polar(fi,shiftedavgd-offset,'y');
Ge=(avga+shiftedavgb+shiftedavgc+shiftedavgd)/4;
Gee=max(Ge)-min(Ge);
polar(fi,Ge-offset,'k');
title(Gee);
legend('avga','shiftedavgb','shiftedavgc','shiftedavgd','Ge')
```

Appendix C: The MATLAB script of upside-down method to evaluate all angles of the cylinder standard

```
close all;
clear all;
%First read data files
r1=Read_txt_offset15('CYL1-01.TXT');
r2=Read_txt_offset15('CYL1-02.TXT');
r3=Read_txt_offset15('CYL1-03.TXT');
r4=Read_txt_offset15('CYL1-04.TXT');
r5=Read_txt_offset15('CYL1-05.TXT');
r6=Read_txt_offset15('CYL1-06.TXT');
r7=Read_txt_offset15('CYL1-07.TXT');
r8=Read_txt_offset15('CYL1-08.TXT');
r9=Read_txt_offset15('CYL1-09.TXT');
r10=Read_txt_offset15('CYL1-10.TXT');
r11=Read_txt_offset15('CYL1-11.TXT');
r12=Read_txt_offset15('CYL1-12.TXT');
r13=Read_txt_offset15('CYL1-13.TXT');
r14=Read_txt_offset15('CYL1-14.TXT');
r15=Read_txt_offset15('CYL1-15.TXT');
r16=Read_txt_offset15('CYL1-16.TXT');
r17=Read_txt_offset15('CYL1-17.TXT');
r18=Read_txt_offset15('CYL1-18.TXT');
r19=Read_txt_offset15('CYL1-19.TXT');
r20=Read_txt_offset15('CYL1-20.TXT');
r21=Read_txt_offset15('CYL1-21.TXT');
% Then read upside down data
rud1=Read_txt_offset15('CYUD1-01.TXT');
rud2=Read_txt_offset15('CYUD1-02.TXT');
rud3=Read_txt_offset15('CYUD1-03.TXT');
rud4=Read_txt_offset15('CYUD1-04.TXT');
rud5=Read_txt_offset15('CYUD1-05.TXT');
rud6=Read_txt_offset15('CYUD1-06.TXT');
rud7=Read_txt_offset15('CYUD1-07.TXT');
rud8=Read_txt_offset15('CYUD1-08.TXT');
rud9=Read_txt_offset15('CYUD1-09.TXT');
rud10=Read_txt_offset15('CYUD1-10.TXT');
rud11=Read_txt_offset15('CYUD1-11.TXT');
rud12=Read_txt_offset15('CYUD1-12.TXT');
rud13=Read_txt_offset15('CYUD1-13.TXT');
rud14=Read_txt_offset15('CYUD1-14.TXT');
rud15=Read_txt_offset15('CYUD1-15.TXT');
rud16=Read_txt_offset15('CYUD1-16.TXT');
rud17=Read_txt_offset15('CYUD1-17.TXT');
rud18=Read_txt_offset15('CYUD1-18.TXT');
rud19=Read_txt_offset15('CYUD1-19.TXT');
rud20=Read_txt_offset15('CYUD1-20.TXT');
rud21=Read_txt_offset15('CYUD1-21.TXT');
% using the for loop function to execute array creation in a loop for
3600 times, generate 3600 vertical lines (generatrix) for all data
for i=1:3600
    Gen0(i,:)=[r1(1*i) r2(1*i) r3(1*i) r4(1*i) r5(1*i) r6(1*i) r7(1*i)
r8(1*i) r9(1*i) r10(1*i) r11(1*i) r12(1*i) r13(1*i) r14(1*i) r15(1*i)
```

```
r16(1*i) r17(1*i) r18(1*i) r19(1*i) r20(1*i) r21(1*i)]/1000;
Genud0(i,:)=[rud1(1*i) rud2(1*i) rud3(1*i) rud4(1*i) rud5(1*i)
rud6(1*i) rud7(1*i) rud8(1*i) rud9(1*i) rud10(1*i) rud11(1*i)
rud12(1*i) rud13(1*i) rud14(1*i) rud15(1*i) rud16(1*i) rud17(1*i)
rud18(1*i) rud19(1*i) rud20(1*i) rud21(1*i)]/1000;
end
height=[12.5 36.4 60.3 84.2 108.1 132 155.9 179.8 203.7 227.6 251.5
275.4 299.3 323.2 347.1 371 394.9 418.8 442.7 466.6 490.5];
%apply least squares fit to all vertical lines
p0 = arrayfun(@(i) polyfit(Gen0(i,:), height, 1), 1:size(Gen0,1),
'UniformOutput', false);
pud0 = arrayfun(@(i) polyfit(Genud0(i,:), height, 1),
1:size(Genud0,1), 'UniformOutput', false);
% calculate average of all slopes and offsets
p0mat = cell2mat(p0')';
slope_average=mean(p0mat(1,:));
offset_average=mean(p0mat(2,:));
plot(Gen0,height,'b'); hold on
x=[min(min(Gen0)),max(max(Gen0))];
y = slope_average * x + offset_average;
plot(x,y,'b');
xlabel('Run-out / mm')
ylabel('Height / mm')
xlabel('Run-out / mm', 'FontSize', 14);
ylabel('Height / mm', 'FontSize', 14);
set(gca, 'FontSize', 12);

%calculate average of all slopes and offsets for upside-down data
pud0mat = cell2mat(pud0')';
slopeud_average=mean(pud0mat(1,:));
offsetud_average=mean(pud0mat(2,:));
figure
plot(Genud0,height,'b');
hold on
xud=[min(min(Genud0)),max(max(Genud0))];
yud = slopeud_average * xud + offsetud_average;
plot(xud,yud,'r');
xlabel('Run-out / mm')
ylabel('Height / mm')
xlabel('Run-out / mm', 'FontSize', 14);
ylabel('Height / mm', 'FontSize', 14);
set(gca, 'FontSize', 12);

% then from slope to angle
angle0=rad2deg(atan(slope_average));
tilt_angle=90-angle0;
angleud0=rad2deg(atan(slopeud_average));
tilt_angleud=90-angleud0;
tilt_anglefinal=(tilt_angle+tilt_angleud)/2
```

Appendix D: The MATLAB script to evaluate column straightness error using the straightness standard

```
close all;
clear all;
r1=Read_txt('STR13.TXT');
r2=Read_txt('STR14.TXT')*1000;
r3=Read_txt('STR15.TXT');
r4=Read_txt('STR16.TXT');
r5=Read_txt('STR17.TXT');

ravg=(r1+r2+r3+r4+r5)/5;
% Generate height vector from 18.5 to 503.11 with 1979 points
height = linspace(18.5, 503.11, 1979);

% Remove the first and last few points
start_index = 100; % Adjust this value to change the number of points
to remove from the start
end_index = length(height) - 100; % Adjust this value to change the
number of points to remove from the end
% Plot data using height as y-axis
plot(ravg(start_index:end_index), height(start_index:end_index), 'b');
hold on
% Get the fitting line for the average line
p=polyfit(ravg(start_index:end_index),height(start_index:end_in-
dex),1);
plot(ravg(start_index:end_index),polyval(p,ravg(start_index:end_in-
dex)),'r');
xlabel(' Measured Straightness deviation (μm)')
ylabel('Height (mm)')
% change the x, y of the fitting line, and then can calculate the de-
viation
p0 = polyfit(height(start_index:end_index), ravg(start_index:end_in-
dex),1);
fit_line = polyval(p0, height(start_index:end_index));

figure
% Calculate the deviation between the fitting line and the original
line
deviation = ravg(start_index:end_index) - fit_line;
% Plot the deviation
plot(deviation, height(start_index:end_index), 'k');
xlabel(' Measured Straightness deviation (μm)')
ylabel('Height (mm)')
figure
plot(height(start_index:end_index) ,deviation, 'k');
xlabel('Height (mm)')
ylabel(' Measured Straightness deviation (μm)')
hold on
countByFifty=50:25:450;
plot(countByFifty,-straightness(countByFifty),'+');
```

The MATLAB script of the `straightness` function

```
function str_comp = straightness(x)
% Returns compensation for straightness error at heigth x, z is help-
ful
% variable
z = (x-260.7)/125.9;
str_error = -0.03788*z.^9 - 0.05796*z.^8 + 0.2922*z.^7 + 0.3836*z.^6 -
0.8089*z.^5 - 0.8126*z.^4 + 0.9132*z.^3 + 0.7696*z.^2 - 0.3169*z -
0.2647;
str_comp=-str_error;
```

Appendix E: The MATLAB script to compensate the angle error and straight error

```
%Example of compensation for the angle error and straight error
close all;
clear all;
%First read data files
r1=Read_txt_offset15('CYL1-01.TXT');
r2=Read_txt_offset15('CYL1-02.TXT');
r3=Read_txt_offset15('CYL1-03.TXT');
r4=Read_txt_offset15('CYL1-04.TXT');
r5=Read_txt_offset15('CYL1-05.TXT');
r6=Read_txt_offset15('CYL1-06.TXT');
r7=Read_txt_offset15('CYL1-07.TXT');
r8=Read_txt_offset15('CYL1-08.TXT');
r9=Read_txt_offset15('CYL1-09.TXT');
r10=Read_txt_offset15('CYL1-10.TXT');
r11=Read_txt_offset15('CYL1-11.TXT');
r12=Read_txt_offset15('CYL1-12.TXT');
r13=Read_txt_offset15('CYL1-13.TXT');
r14=Read_txt_offset15('CYL1-14.TXT');
r15=Read_txt_offset15('CYL1-15.TXT');
r16=Read_txt_offset15('CYL1-16.TXT');
r17=Read_txt_offset15('CYL1-17.TXT');
r18=Read_txt_offset15('CYL1-18.TXT');
r19=Read_txt_offset15('CYL1-19.TXT');
r20=Read_txt_offset15('CYL1-20.TXT');
r21=Read_txt_offset15('CYL1-21.TXT');

height=[12.5 36.4 60.3 84.2 108.1 132 155.9 179.8 203.7 227.6 251.5
275.4 299.3 323.2 347.1 371 394.9 418.8 442.7 466.6 490.5];

n=3600;
i=1:n;
fi=(i/n*2*pi);
% polar(fi,r5);
% hold on
% polar(fi,r2);
one=ones(3600,1);
[x1,y1,z1] = pol2cart(fi,r1,12.5*one);
plot3(x1,y1,z1); hold on;
[x2,y2,z2] = pol2cart(fi,r2,36.4*one);
plot3(x2,y2,z2);
[x3,y3,z3] = pol2cart(fi,r3,60.3*one);
plot3(x3,y3,z3);
[x4,y4,z4] = pol2cart(fi,r4,84.2*one);
plot3(x4,y4,z4);
[x5,y5,z5] = pol2cart(fi,r5,108.1*one);
plot3(x5,y5,z5);
[x6,y6,z6] = pol2cart(fi,r6,132*one);
plot3(x6,y6,z6);
[x7,y7,z7] = pol2cart(fi,r7,155.9*one);
plot3(x7,y7,z7);
```

```
[x8,y8,z8] = pol2cart(fi,r8,179.8*one);
plot3(x8,y8,z8);
[x9,y9,z9] = pol2cart(fi,r9,203.7*one);
plot3(x9,y9,z9);
[x10,y10,z10] = pol2cart(fi,r10,227.6*one);
plot3(x10,y10,z10);
[x11,y11,z11] = pol2cart(fi,r11,251.5*one);
plot3(x11,y11,z11);
[x12,y12,z12] = pol2cart(fi,r12,275.4*one);
plot3(x12,y12,z12);
[x13,y13,z13] = pol2cart(fi,r13,299.3*one);
plot3(x13,y13,z13);
[x14,y14,z14] = pol2cart(fi,r14,323.2*one);
plot3(x14,y14,z14);
[x15,y15,z15] = pol2cart(fi,r15,347.1*one);
plot3(x15,y15,z15);
[x16,y16,z16] = pol2cart(fi,r16,371*one);
plot3(x16,y16,z16);
[x17,y17,z17] = pol2cart(fi,r17,394.9*one);
plot3(x17,y17,z17);
[x18,y18,z18] = pol2cart(fi,r18,418.8*one);
plot3(x18,y18,z18);
[x19,y19,z19] = pol2cart(fi,r19,442.7*one);
plot3(x19,y19,z19);
[x20,y20,z20] = pol2cart(fi,r20,466.6*one);
plot3(x20,y20,z20);
[x21,y21,z21] = pol2cart(fi,r21,490.5*one);
plot3(x21,y21,z21);
xlabel('Deviation-x / µm')
ylabel('Deviation-y / µm')
zlabel('Height-z / mm')
xlabel('Deviation-x / µm', 'FontSize', 14);
ylabel('Deviation-y / µm', 'FontSize', 14);
zlabel('Height / mm', 'FontSize', 14);
set(gca, 'FontSize', 12);

%compensated data is defined by the results added by the angle compen-
sation
%and straightness compensation
r1_comp=r1+angle(height(1))+straightness(height(1));
r2_comp=r2+angle(height(2))+straightness(height(2));
r3_comp=r3+angle(height(3))+straightness(height(3));
r4_comp=r4+angle(height(4))+straightness(height(4));
r5_comp=r5+angle(height(5))+straightness(height(5));
r6_comp=r6+angle(height(6))+straightness(height(6));
r7_comp=r7+angle(height(7))+straightness(height(7));
r8_comp=r8+angle(height(8))+straightness(height(8));
r9_comp=r9+angle(height(9))+straightness(height(9));
r10_comp=r10+angle(height(10))+straightness(height(10));
r11_comp=r11+angle(height(11))+straightness(height(11));
r12_comp=r12+angle(height(12))+straightness(height(12));
r13_comp=r13+angle(height(13))+straightness(height(13));
r14_comp=r14+angle(height(14))+straightness(height(14));
r15_comp=r15+angle(height(15))+straightness(height(15));
```

```
r16_comp=r16+angle(height(16))+straightness(height(16));
r17_comp=r17+angle(height(17))+straightness(height(17));
r18_comp=r18+angle(height(18))+straightness(height(18));
r19_comp=r19+angle(height(19))+straightness(height(19));
r20_comp=r20+angle(height(20))+straightness(height(20));
r21_comp=r21+angle(height(21))+straightness(height(21));
figure
[X1,Y1,Z1] = pol2cart(fi,r1_comp,12.5*one);
plot3(X1,Y1,Z1); hold on;
[X2,Y2,Z2] = pol2cart(fi,r2_comp,36.4*one);
plot3(X2,Y2,Z2);
[X3,Y3,Z3] = pol2cart(fi,r3_comp,60.3*one);
plot3(X3,Y3,Z3);
[X4,Y4,Z4] = pol2cart(fi,r4_comp,84.2*one);
plot3(X4,Y4,Z4);
[X5,Y5,Z5] = pol2cart(fi,r5_comp,108.1*one);
plot3(X5,Y5,Z5);
[X6,Y6,Z6] = pol2cart(fi,r6_comp,132*one);
plot3(X6,Y6,Z6);
[X7,Y7,Z7] = pol2cart(fi,r7_comp,155.9*one);
plot3(X7,Y7,Z7);
[X8,Y8,Z8] = pol2cart(fi,r8_comp,179.8*one);
plot3(X8,Y8,Z8);
[X9,Y9,Z9] = pol2cart(fi,r9_comp,203.7*one);
plot3(X9,Y9,Z9);
[X10,Y10,Z10] = pol2cart(fi,r10_comp,227.6*one);
plot3(X10,Y10,Z10);
[X11,Y11,Z11] = pol2cart(fi,r11_comp,251.5*one);
plot3(X11,Y11,Z11);
[X12,Y12,Z12] = pol2cart(fi,r12_comp,275.4*one);
plot3(X12,Y12,Z12);
[X13,Y13,Z13] = pol2cart(fi,r13_comp,299.3*one);
plot3(X13,Y13,Z13);
[X14,Y14,Z14] = pol2cart(fi,r14_comp,323.2*one);
plot3(X14,Y14,Z14);
[X15,Y15,Z15] = pol2cart(fi,r15_comp,347.1*one);
plot3(X15,Y15,Z15);
[X16,Y16,Z16] = pol2cart(fi,r16_comp,371*one);
plot3(X16,Y16,Z16);
[X17,Y17,Z17] = pol2cart(fi,r17_comp,394.9*one);
plot3(X17,Y17,Z17);
[X18,Y18,Z18] = pol2cart(fi,r18_comp,418.8*one);
plot3(X18,Y18,Z18);
[X19,Y19,Z19] = pol2cart(fi,r19_comp,442.7*one);
plot3(X19,Y19,Z19);
[X20,Y20,Z20] = pol2cart(fi,r20_comp,466.6*one);
plot3(X20,Y20,Z20);
[X21,Y21,Z21] = pol2cart(fi,r21_comp,490.5*one);
plot3(X21,Y21,Z21);

% Test for Least Squares fitting case with 21 planes
Angles=[fi fi fi fi fi fi fi fi fi fi fi fi fi fi fi fi fi fi fi fi
fi];
```

```
H1=(height(1)*one)';
H2=(height(2)*one)';
H3=(height(3)*one)';
H4=(height(4)*one)';
H5=(height(5)*one)';
H6=(height(6)*one)';
H7=(height(7)*one)';
H8=(height(8)*one)';
H9=(height(9)*one)';
H10=(height(10)*one)';
H11=(height(11)*one)';
H12=(height(12)*one)';
H13=(height(13)*one)';
H14=(height(14)*one)';
H15=(height(15)*one)';
H16=(height(16)*one)';
H17=(height(17)*one)';
H18=(height(18)*one)';
H19=(height(19)*one)';
H20=(height(20)*one)';
H21=(height(21)*one)';
Heights=[H1 H2 H3 H4 H5 H6 H7 H8 H9 H10 H11 H12 H13 H14 H15 H16 H17
H18 H19 H20 H21];
R=[r1_comp r2_comp r3_comp r4_comp r5_comp r6_comp r7_comp r8_comp
r9_comp r10_comp r11_comp r12_comp r13_comp r14_comp r15_comp r16_comp
r17_comp r18_comp r19_comp r20_comp r21_comp];
M=[Angles' Heights' R'];
[r, a, b, e, f] = Limacoid(M)

% Centering using ecentricity values
r1c=r1_comp+(a+height(1)*e)*cos(fi)+(b+height(1)*f)*sin(fi);
r2c=r2_comp+(a+height(2)*e)*cos(fi)+(b+height(2)*f)*sin(fi);
r3c=r3_comp+(a+height(3)*e)*cos(fi)+(b+height(3)*f)*sin(fi);
r4c=r4_comp+(a+height(4)*e)*cos(fi)+(b+height(4)*f)*sin(fi);
r5c=r5_comp+(a+height(5)*e)*cos(fi)+(b+height(5)*f)*sin(fi);
r6c=r6_comp+(a+height(6)*e)*cos(fi)+(b+height(6)*f)*sin(fi);
r7c=r7_comp+(a+height(7)*e)*cos(fi)+(b+height(7)*f)*sin(fi);
r8c=r8_comp+(a+height(8)*e)*cos(fi)+(b+height(8)*f)*sin(fi);
r9c=r9_comp+(a+height(9)*e)*cos(fi)+(b+height(9)*f)*sin(fi);
r10c=r10_comp+(a+height(10)*e)*cos(fi)+(b+height(10)*f)*sin(fi);
r11c=r11_comp+(a+height(11)*e)*cos(fi)+(b+height(11)*f)*sin(fi);
r12c=r12_comp+(a+height(12)*e)*cos(fi)+(b+height(12)*f)*sin(fi);
r13c=r13_comp+(a+height(13)*e)*cos(fi)+(b+height(13)*f)*sin(fi);
r14c=r14_comp+(a+height(14)*e)*cos(fi)+(b+height(14)*f)*sin(fi);
r15c=r15_comp+(a+height(15)*e)*cos(fi)+(b+height(15)*f)*sin(fi);
r16c=r16_comp+(a+height(16)*e)*cos(fi)+(b+height(16)*f)*sin(fi);
r17c=r17_comp+(a+height(17)*e)*cos(fi)+(b+height(17)*f)*sin(fi);
r18c=r18_comp+(a+height(18)*e)*cos(fi)+(b+height(18)*f)*sin(fi);
r19c=r19_comp+(a+height(19)*e)*cos(fi)+(b+height(19)*f)*sin(fi);
r20c=r20_comp+(a+height(20)*e)*cos(fi)+(b+height(20)*f)*sin(fi);
r21c=r21_comp+(a+height(21)*e)*cos(fi)+(b+height(21)*f)*sin(fi);

arr=[r1c, r2c, r3c, r4c, r5c, r6c, r7c, r8c, r9c, r10c, r11c, r12c,
r13c, r14c, r15c, r16c, r17c, r18c, r19c,r20c, r21c];
```

```
S=min(arr);
L=max(arr);
CYLt=L-S
figure
[A1,B1,C1] = pol2cart(fi,r1c,height(1)*one);
plot3(A1,B1,C1);hold on
[A2,B2,C2] = pol2cart(fi,r2c,height(2)*one);
plot3(A2,B2,C2);
[A3,B3,C3] = pol2cart(fi,r3c,height(3)*one);
plot3(A3,B3,C3);
[A4,B4,C4] = pol2cart(fi,r4c,height(4)*one);
plot3(A4,B4,C4);
[A5,B5,C5] = pol2cart(fi,r5c,height(5)*one);
plot3(A5,B5,C5);
[A6,B6,C6] = pol2cart(fi,r6c,height(6)*one);
plot3(A6,B6,C6);
[A7,B7,C7] = pol2cart(fi,r7c,height(7)*one);
plot3(A7,B7,C7);
[A8,B8,C8] = pol2cart(fi,r8c,height(8)*one);
plot3(A8,B8,C8);
[A9,B9,C9] = pol2cart(fi,r9c,height(9)*one);
plot3(A9,B9,C9);
[A10,B10,C10] = pol2cart(fi,r10c,height(10)*one);
plot3(A10,B10,C10);
[A11,B11,C11] = pol2cart(fi,r11c,height(11)*one);
plot3(A11,B11,C11);
[A12,B12,C12] = pol2cart(fi,r12c,height(12)*one);
plot3(A12,B12,C12);
[A13,B13,C13] = pol2cart(fi,r13c,height(13)*one);
plot3(A13,B13,C13);
[A14,B14,C14] = pol2cart(fi,r14c,height(14)*one);
plot3(A14,B14,C14);
[A15,B15,C15] = pol2cart(fi,r15c,height(15)*one);
plot3(A15,B15,C15);
[A16,B16,C16] = pol2cart(fi,r16c,height(16)*one);
plot3(A16,B16,C16);
[A17,B17,C17] = pol2cart(fi,r17c,height(17)*one);
plot3(A17,B17,C17);
[A18,B18,C18] = pol2cart(fi,r18c,height(18)*one);
plot3(A18,B18,C18);
[A19,B19,C19] = pol2cart(fi,r19c,height(19)*one);
plot3(A19,B19,C19);
[A20,B20,C20] = pol2cart(fi,r20c,height(20)*one);
plot3(A20,B20,C20);
[A21,B21,C21] = pol2cart(fi,r21c,height(21)*one);
plot3(A21,B21,C21);
xlabel('Deviation-x / µm')
ylabel('Deviation-y / µm')
zlabel('Height-z / mm')
xlabel('Deviation-x / µm', 'FontSize', 14);
ylabel('Deviation-y / µm', 'FontSize', 14);
zlabel('Height / mm', 'FontSize', 14);
set(gca, 'FontSize', 12);
```

The MATLAB script of the function angle

```
function angle_comp = angle(x)
% Returns compensation for column angle error at height x
rad = deg2rad(0.00060);
angle_comp=-x*rad*1000;    % Outward error correct into the inward
compensation
```